Article

Developmental Cell

The Arabidopsis Receptor Kinase IRK Is Polarized and Represses Specific Cell Divisions in Roots

Graphical Abstract

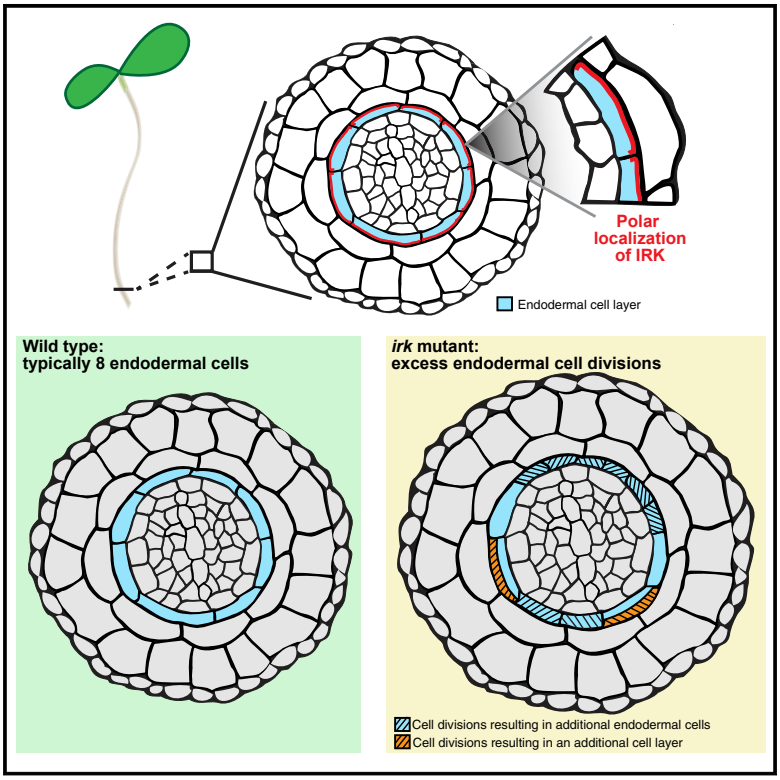

Authors

Roya Campos, Jason Goff, Cecilia Rodriguez-Furlan, Jaimie M. Van Norman

Correspondence

jaimie.vannorman@ucr.edu

In Brief

Coordination of cell division across tissues and organs is fundamental to development in multicellular eukaryotes. Campos et al. identify IRK, a transmembrane receptor kinase with polar localization that negatively regulates specific cell divisions. Therefore, IRK connects signaling and cell polarity with the control of oriented cell divisions during tissue development.

Highlights

- IRK, a transmembrane receptor kinase, is polarly localized in root cells
- In adjacent cell types, IRK is localized to different plasma membrane domains
- Distinct IRK localization patterns are informed locally by adjacent cell types
- IRK functions to inhibit specific cell divisions in the root ground tissue

Campos et al., 2020, Developmental Cell *52*, 183–195
January 27, 2020
https://doi.org/10.1016/j.devcel.2019.12.001

CellPress

Developmental Cell
Article

The Arabidopsis Receptor Kinase IRK Is Polarized and Represses Specific Cell Divisions in Roots

Roya Campos,[1,2] Jason Goff,[1,2] Cecilia Rodriguez-Furlan,[1,2] and Jaimie M. Van Norman[1,2,3,*]
[1]Department of Botany and Plant Sciences, University of California, Riverside, Riverside, CA 92521, USA
[2]Center for Plant Cell Biology, Institute of Integrative Genome Biology, University of California, Riverside, Riverside, CA 92521, USA
[3]Lead Contact
*Correspondence: jaimie.vannorman@ucr.edu
https://doi.org/10.1016/j.devcel.2019.12.001

SUMMARY

Development of multicellular organisms requires coordination of cell division and differentiation across tissues. In plants, directional signaling, and implicitly cell polarity, is proposed to participate in this coordination; however, mechanistic links between intercellular signaling, cell polarity, and cellular organization remain unclear. Here, we investigate the localization and function of *INFLORESCENCE AND ROOT APICES RECEPTOR KINASE* (IRK) in root development. We find that IRK-GFP localizes to the outer plasma membrane domain in endodermal cells but localizes to different domains in other cell types. Our results suggest that IRK localization is informed locally by adjacent cell types. *irk* mutants have excess cell divisions in the ground tissue stem cells and endodermis, indicating IRK functions to maintain tissue organization through inhibition of specific cell divisions. We predict that IRK perceives a directional cue that negatively regulates these cell divisions, thus linking intercellular signaling and cell polarity with the control of oriented cell divisions during development.

INTRODUCTION

Organ patterning requires coordination of cell division and differentiation across distinct cell types and over time. In plants, the spatial relationships between cells are essentially fixed because of the cell wall; as a result, the orientation of plant cell divisions is particularly important for cell fate determination and tissue morphology (Facette et al., 2019; Rasmussen and Bellinger, 2018). In the *Arabidopsis thaliana* root, cellular organization is nearly invariant, maintained by stringent control of the timing and orientation of cell divisions during development (Figures 1A–1C) (Van Norman, 2016; Scheres and Benfey, 1999). Root cell divisions typically occur in three division planes (Figures 1C–1E). Periclinal cell divisions are oriented parallel to the root surface and in the root and are often formative (asymmetric), generating additional cell types. Transverse and longitudinal anticlinal cell divisions are oriented perpendicular to the root surface and are typically proliferative, producing more cells of a given type. During root ground tissue (GT) development, the stem cell—the cortex and endodermal initial (CEI) cell—undergoes a formative, anticlinally oriented cell division to produce a CEI daughter (CEID) (Dolan et al., 1993; Scheres et al., 1995; Benfey et al., 1993). This daughter cell then undergoes a periclinal, formative division to produce two cell types, the endodermis toward the inside and cortex toward the outside. Arabidopsis endodermal cells can then undergo one more periclinally oriented, formative cell division to produce an additional cell layer called the middle (or secondary) cortex (Figure 1F) (Paquette and Benfey, 2005; Baum et al., 2002).

In the root meristem, cell-cell communication provides essential input into formative cell divisions and subsequent cell fate specification during tissue development (Van Norman et al., 2011; Kidner et al., 2000; van den Berg et al., 1995, 1997; Nakajima and Benfey, 2002). The orientation of root formative cell divisions and cell fate specification of the resulting daughter cells are likely based primarily on extrinsic factors. This model is supported by cell ablation studies showing that root stem cell maintenance and daughter cell differentiation, as well as tissue repair following wounding, depend on extrinsic cues (van den Berg et al., 1995, 1997; Kidner et al., 2000; Marhava et al., 2019). Implicit in this model is that perception of these cues, perhaps at the plasma membrane (PM), precede downstream events leading to cell division or differentiation. Informational cues transmitted in the root's radial axis has been established through characterization of mobile transcription factors and microRNAs. For instance, SHORT ROOT (SHR) a key transcriptional regulator of GT formative divisions and endodermal cell identity is expressed in the stele and moves outward to regulate GT developmental events (Helariutta et al., 2000; Gallagher et al., 2004; Koizumi et al., 2012; Nakajima et al., 2001). Additionally, a gradient of microRNA165/166 that originates in the endodermis is required for specification of internal xylem cell types (Carlsbecker et al., 2010; Miyashima et al., 2011). These examples indicate that various types of informational cues originate in one tissue and promote formative divisions and/or differentiation of cells in adjacent tissues across the root's radial axis. Despite the developmental importance of radial intercellular communication across root cell types, the role of signaling across the PM in the radial axis remains largely unknown.

Relatively few polar-localized signaling proteins have been identified in plants. Asymmetric protein distribution at the PM is a common attribute of polarized cells. Cell polarity can be defined as asymmetry in any aspect of development, or physiology, along a single cellular axis. In Arabidopsis root cells, polarized proteins are typically ascribed to one of four regions of the PM (Nakamura and Grebe, 2018; Van Norman, 2016; Łangowski

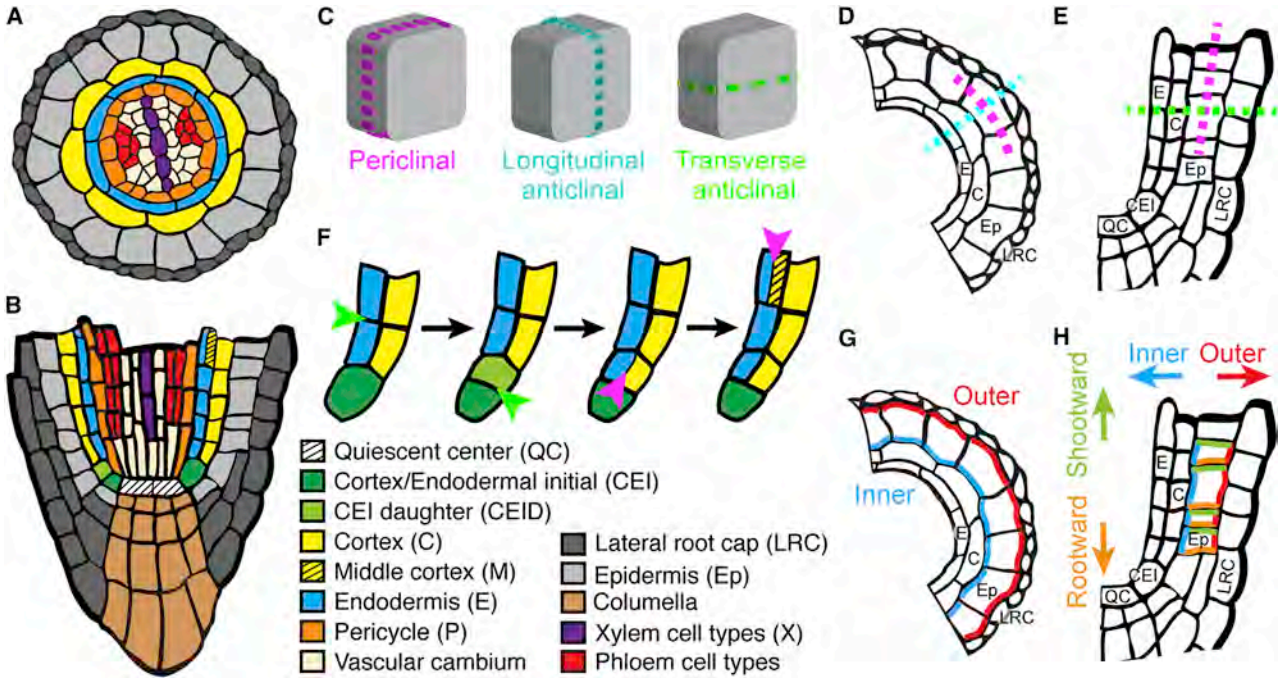

Figure 1. Root Cellular Organization, Division Plane Orientation, and Plasma Membrane Domains

Schematics sections of *Arabidopsis thaliana* root tip (A), (D), and (G) transverse and (B), (E), (F), and (H) median longitudinal. (C–E) Typical division plane orientations (dotted lines) in (C) individual cells and (D) and (E) across the root axes. (F) During GT development, periclinal cell divisions (magenta arrowheads) in the CEID generate the endodermis and cortex, while in the endodermis, the middle cortex is produced. Transverse anticlinal cell divisions (green arrowheads) produce the CEID and more cells within a file, and longitudinal anticlinal cell divisions if present would produce more cells within a ring of cells. (G and H) The four plasma membrane domains across the root axes where polar-localized proteins typically accumulate.

et al., 2016). The shootward and rootward PM domains are oriented toward the shoot or root apices, respectively, and the inner and outer PM domains are oriented toward or away from the root vasculature, respectively (Figures 1G and 1H). There are several examples of developmentally important proteins localizing to the root/shootward PM domains in root cells. The auxin efflux transporters, *PIN*-FORMED (PINs), most often localize to the rootward or shootward PM domains and changes in the direction of auxin transport, mediated by PINs, are important for many developmental processes (Petrásek and Friml, 2009; Wisniewska et al., 2006). The PM-associated proteins BRAVIS RADIX (BRX) and OCTOPUS (OPS) are localized to the rootward and shootward polar domains, respectively, in protophloem cells. These proteins function in phloem development including formative divisions and despite their opposite localization were found to function genetically in parallel. Chimeric protein fusions between BRX and OPS mislocalize to the rootward PM domain but are nonetheless able to rescue *ops* mutants, indicating that shootward localization of OPS is dispensable for its function (Breda et al., 2017; Truernit et al., 2012; Scacchi et al., 2009). Protein localization to the inner/outer PM domains has largely been limited to transporters, such as those involved in the transport of boron. Nutrient transporter polarity is functionally necessary and their directionality is intuitive (Ma et al., 2006, 2007; Takano et al., 2010; Alassimone et al., 2010; Barberon et al., 2014). We predict that proteins involved in the perception and/or transmission of extracellular, directional cues may also be laterally polarized and contribute to signaling across the root's radial axis.

Stomatal development is an example in plants where cell polarity, formative cell divisions, and cellular differentiation are directly linked (Shao and Dong, 2016; Lau and Bergmann, 2012). In Arabidopsis, the polarly localized membrane-associated proteins BASL (Dong et al., 2009), POLAR (Pillitteri et al., 2011), and BRXL2 (Rowe et al., 2019) are required to orient formative cell divisions in the stomatal lineage. However, it is unclear how these proteins localize to specific PM positions, potentially implicating membrane-localized interaction partners. In maize, two transmembrane receptor kinases, PAN1 and PAN2, are polarly localized in the subsidiary cell and required for its asymmetric cell division in stomatal development (Cartwright et al., 2009; Zhang et al., 2012; Facette et al., 2015). PAN1 and PAN2 encode proteins of the transmembrane group of receptor-like kinases (RLKs), which are encoded by a large gene family in plants, each with a series of extracellular leucine-rich repeats (LRR), single transmembrane domain, and cytoplasmic kinase domain (Shiu and Bleecker, 2001, 2003). LRR-RLKs are generally predicted to perceive extracellular ligands and activate downstream signaling pathways.

Among the functionally characterized LRR-RLKs, all but a few function as receptors for peptide ligands. In root tissue development, several LRR-RLK-peptide pairs have been identified. For example, PHLOEM INTERCALATED WITH XYLEM (PXY) perceives CLAVATA3/EMBRYO SURROUNDING REGION 41 (CLE41) and CLE44 to regulate vascular tissue development (Etchells et al., 2016; Etchells and Turner, 2010; Morita et al., 2016; Hirakawa et al., 2008). The CLE9/10 peptides regulate

periclinal cell divisions during xylem development via the BARELY NO MERISTEM (BAM) receptor kinase family, and CLE45 suppresses aspects of phloem development through BAM3 (Qian et al., 2018; Depuydt et al., 2013). Modulation of root cap sloughing and formation of new root cap cell layers requires the signaling pair HAESA-LIKE2 and the INFLORESCENCE DEFICIENT IN ABSCISSION-LIKE1 (IDL1) peptide (Shi et al., 2018). Endodermal differentiation requires the SCHENGEN3 (SGN3) receptor together with the CASPARIAN STRIP INTEGRITY FACTORS (CIF1/2) for formation of the Casparian strip (Doblas et al., 2017; Okuda et al., 2019). Despite these and a few other well characterized examples, the vast majority of LRR-RLKs remain functionally uncharacterized with unknown ligands.

We proposed that proteins functioning in signaling and root patterning could be identified via cell-type-specific expression. Toward this end, we identified a set of LRR-RLKs we termed polarly localized kinases (PLKs) that accumulate to specific PM domains in various cell types. Here, we report a detailed characterization of one PLK named INFLORESCENCE AND ROOT APICES RECEPTOR KINASE (IRK) that is polarly localized in GT and required for its patterning . We find that IRK-GFP is localized to distinct PM domains in different cell types, a unique feature among characterized Arabidopsis LRR-RLKs. Specifically, IRK-GFP localizes to the outer PM domain in the endodermis and exhibits polar or nonpolar localization in other cell types. Based on this cell type-specific localization, we predicted that cell identity determined IRK localization; however, our data suggest its localization depends on information from radially adjacent cells. We also show that IRK is required to negatively regulate periclinal and longitudinal anticlinal cell divisions (LADs) in the GT lineage. Excess LADs in *irk* mutants results in endodermal cell proliferation in the radial axis. Overall, we propose that IRK functions in a directional signaling pathway that negatively regulates specific GT cell divisions during root development.

RESULTS

IRK Is Localized to Distinct PM Domains in Different Cell Types

We identified IRK (At3g56370) as a candidate protein involved in signaling and formative cell divisions in the root based on its expression in the endodermis and upon SHR induction (Birnbaum et al., 2003; Brady et al., 2007; Li et al., 2016; Sozzani et al., 2010). Consistent with previously reported expression of *IRK* in the root apical meristem (Kanamoto et al., 2002), our transcriptional reporter (*pIRK:erGFP*) showed *IRK* promoter activity predominantly in CEI, CEID, endodermis, pericycle, and some (pro)vascular cell types in the stele. Occasionally, *pIRK* activity was weakly detected in the first few cortical cells but was not detectable in the quiescent center (QC), epidermis, columella, or lateral root cap (Figures 2A–2C).

To examine IRK protein localization, we expressed an IRK-GFP fusion under *pIRK* (*pIRK:IRK:GFP*). In wild type (WT) roots, IRK-GFP is predominantly detected in the CEI, CEID, endodermis, and pericycle (Figures 2D–2I, 2R, and 2S). Although *pIRK* activity was not detected in cell types external to the endodermis, IRK-GFP was weakly detected in cortical and/or epidermal cells. Hyperosmotic treatments in the presence of cellulase better delineated the distinct GFP signal residing in the endodermis, cortex, and epidermis. Upon treatment, IRK-GFP polar distribution is lost and the signal is detected in multiple cell types (Figure S1C). Close examination showed IRK-GFP was not uniformly distributed in the PM of these cell types (Figures 2H and 2I) and localized to the outer PM domains of the endodermis and pericycle. Notably, IRK-GFP localized to the rootward and/or shootward PM domains in the CEI and CEID (Figures 2E, 2H, 2I, and 2R). Furthermore, IRK-GFP localization appeared nonpolar in the middle cortex (Figure 2G). This localization pattern was also observed in the embryonic GT (Figures S1A, S1B, and S1F), indicating IRK-GFP localization is established during embryogenesis and maintained after germination. Together, these results indicate that IRK is a polarly localized LRR-RLK that accumulates at different PM domains in distinct cell types and suggest its localization depends on cell identity.

Ectopic Expression Confirms IRK Localization to Different PM Domains

To eliminate potentially overlapping fluorescent signal from adjacent cell types (e.g., Alassimone et al., 2010), we examined IRK-GFP localization upon expression in individual root cell layers. IRK-GFP expressed from the *SCARECROW* promoter (*pSCR*), which is specifically expressed in the endodermis, CEI, CEID, and QC (Figures 2J–2L) (Wysocka-Diller et al., 2000; Levesque et al., 2006) revealed striking polar localization of IRK-GFP to the outer PM domain of endodermal cells (Figures 2M–2Q, 2T, 2U, and S1E). IRK-GFP localization is also detected at the outward edges of the shootward and rootward domains (Figures 2P and 2Q). In the CEI and CEID, IRK-GFP localizes to the shootward and/or rootward PM domains, and after recent periclinal CEID division, IRK-GFP is not immediately detected in the new PM. This suggests that polar accumulation of IRK-GFP in the endodermis is not due to its presence in the periclinally oriented cell plates of the CEID but is polarly localized upon completion of cytokinesis. Finally, upon misexpression in the QC, IRK-GFP was observed at both the inner and outer PM domains (Figures 2P, 2Q, and S1E). Hyperosmotic treatments in the presence of cellulase revealed that IRK-GFP closely interacts with the endodermal cell wall and suggests that interaction with the cell wall may contribute to the stability of IRK localization upon plasmolysis (Figure S1E). Cell layer-specific expression of IRK-GFP clearly demonstrated its unique localization in the GT initial and endodermal cells.

We also examined IRK-GFP localization upon misexpression in the cortex, epidermis and lateral root cap, using the promoters of *CORTEX2* (*pCO2*) and *WEREWOLF* (*pWER*) (Figures 3A, 3B, 3G, and 3H) (Lee and Schiefelbein, 1999; Heidstra et al., 2004; Paquette and Benfey, 2005). In contrast to the endodermis, IRK-GFP in these cell types is unexpectedly localized to the inner PM domain (Figures 3C, 3D, 3I–3L, and S1D). Consistent with IRK-GFP localization under its own promoter, we observed nonpolar localization of IRK-GFP in the middle cortex of roots expressing *pCO2:IRK:GFP* (Figures 3E and 3F). This indicates that nonpolar IRK-GFP localization in the middle cortex is not dependent on its expression in the endodermal mother cell or localization to that periclinal cell plate. Notably, IRK-GFP did not accumulate in the lateral root cap when expressed by *pWER*, suggesting that IRK may be subject to post-transcriptional regulation.

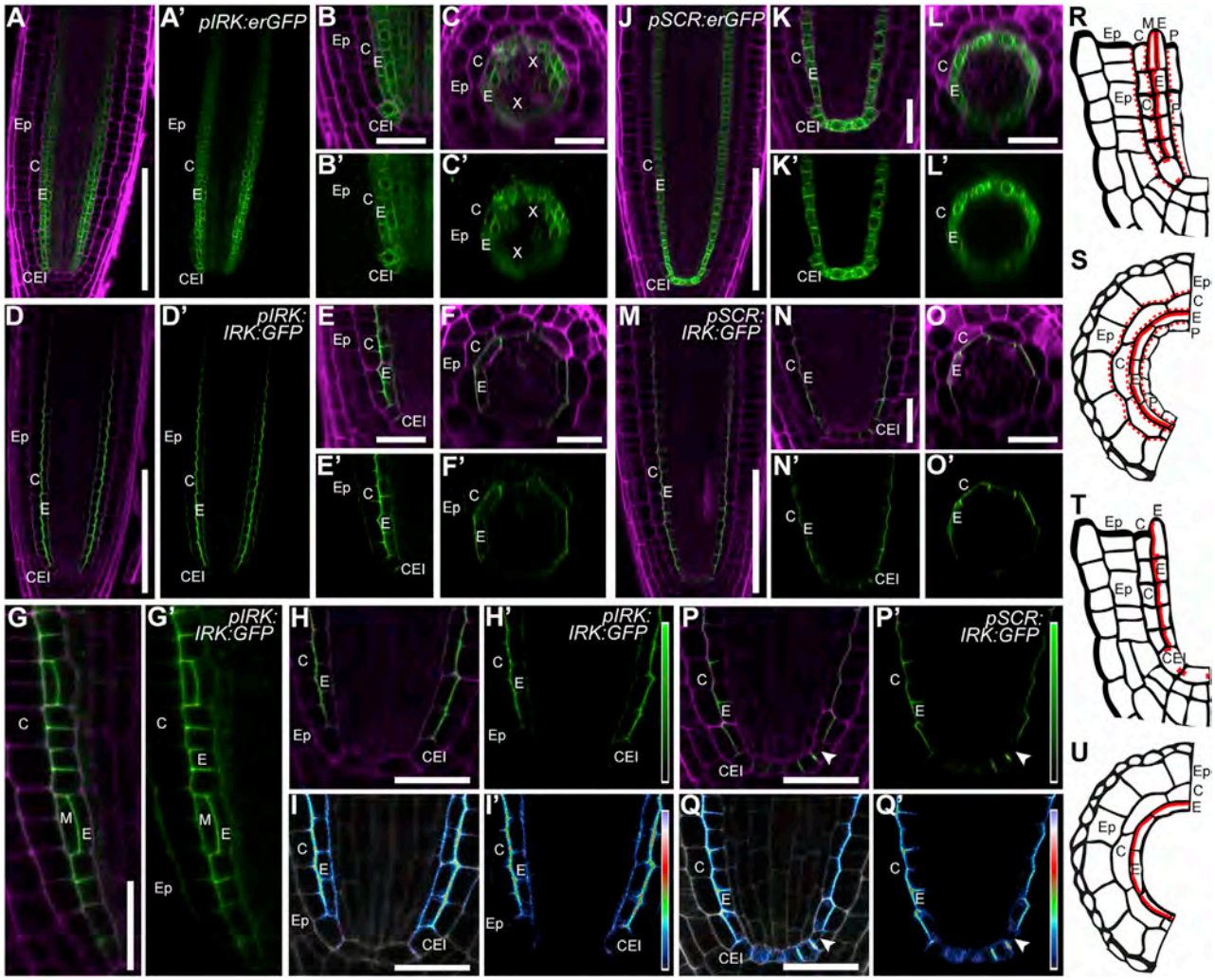

Figure 2. IRK-GFP Predominately Accumulates in Endodermal and Ground Tissue Initial Cells, Where It Is Polarly Localized

(A–Q) Confocal images of WT roots (4–5 dps) expressing green fluorescent protein (GFP) and stained with propidium iodide (PI) to show cell outlines. Adjacent panels show PI + GFP merged (α) and GFP alone (α'). (A–C) Expression of *pIRK:erGFP*. (D–I) Localization of IRK-GFP driven by *pIRK*. (J–L) Expression of *pSCARECROW:erGFP* (*pSCR:erGFP*). (M–Q) IRK-GFP driven by *pSCR*. (I and Q) Intensity color scale (black = low and green or purple = high) to accentuate GFP signal values (identical scales for each genotype (white arrowhead indicates a recent periclinal CEID division).

(R–U) Schematics summarizing IRK-GFP localization (red) driven by *pIRK* in (R) and (S) and *pSCR* in (T) and (U). Dotted lines represent weaker GFP signal. Abbreviations are as follows: CEI, cortex and endodermis initial; E, endodermis; C, cortex; M, middle cortex; Ep, epidermis; X, xylem axis; and P, pericycle. Scale bars: 100 μm in (A), (D), (J), and (M) and 20μm in all others.

See also Figure S1.

Our data indicate that IRK-GFP localization to specific PM domains varies among root cell types and may be informed by cell identity (intrinsic cues), extrinsic cues, or both.

IRK Localization Is Influenced by Adjacent Cells

To examine the influence of cell identity on IRK localization in the GT lineage, we expressed *pCO2:IRK:GFP* in *short root (shr)* and *scarecrow (scr)* mutants, which have defects in GT patterning and cell fate specification. *shr* mutants have a single layer of GT with cortex identity based on reporter expression (Figure 4A) and the absence of detectable endodermal features (Scheres et al., 1995; Helariutta et al., 2000; Nakajima et al., 2001). In *scr* mutants, the single GT layer is described as having mutant or mixed cell identity as it expresses cortex-specific reporters and exhibits endodermal features such as periclinal cell division to produce another GT layer (Figure 4E) (Paquette and Benfey, 2005; Scheres et al., 1995; Di Laurenzio et al., 1996; Wysocka-Diller et al., 2000). We hypothesized that if cell identity was sufficient to direct IRK-GFP to specific PM domains, then it would localize to the inner PM domain of cortical cells in *shr*, as it does in WT and that localization in *scr* would be distinct from *shr* and WT because of the mixed identity of this cell layer.

In the *shr* GT, IRK-GFP localized to the shootward and/or rootward PM domains (Figure 4B, inset). Strikingly, localization of IRK-GFP is centered within these domains (Figures 4B–4D). In the single GT layer of *scr* roots, IRK-GFP also localized to the

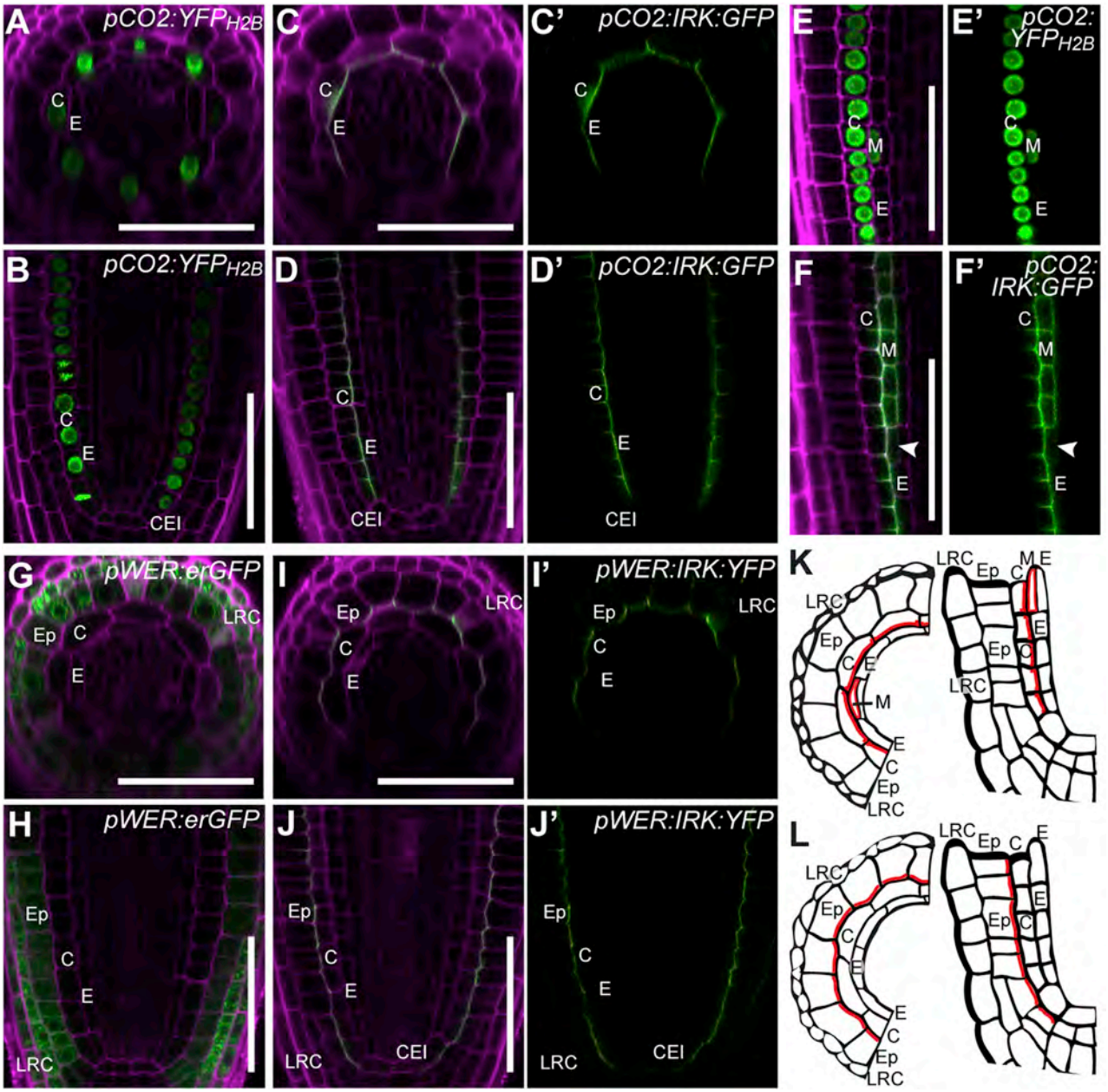

Figure 3. In the Cortex and Epidermis, IRK-GFP Is Localized to the Inner PM Domain

(A–J) Confocal images of WT roots (5 dps) expressing fluorescent proteins (FP, green) and stained with PI (magenta). Adjacent panels show PI + FP merged (α) and FP alone (α'). (A, B, and E) Expression of *pCO2:YFP$_{H2B}$*. (C, D, and F) IRK-GFP driven by *pCO2*. (G and H) Expression of *pWER:erGFP* in the lateral root cap and epidermis. (I and J) IRK-YFP driven by *pWER*.

(K and L) Schematics summarizing IRK-FP localization in the cortex and middle cortex (K) and epidermis (L).

Abbreviations are as follows: E, endodermis; C, cortex; M, middle cortex; Ep, epidermis; and LRC, lateral root cap. Scale bars, 50 μm.

See also Figure S1.

center of the rootward and/or shootward PM domains (Figures 4F–4H). In the PMs formed from recent transverse anticlinal cell divisions (Figure 4F, inset), IRK-GFP appears more evenly distributed suggesting it becomes more centrally localized over time. Additionally, we noticed that in GT cells immediately adjacent to the (presumed) QC, IRK-GFP is detectable only at the shootward PM domain (Figures 4B and 4F, asterisks), whereas localization appears to be at both the rootward and shootward PM domains in more distal cells. IRK-GFP localization in the GT of these mutants is similar to that observed in the CEI and CEID of WT roots.

Intriguingly, after periclinal cell division in the single GT layer in *scr*, IRK-GFP localization is laterally polar (Figure 4F, inset). Because *pCO2* is active in both *scr* GT cell layers (Figure 4E)

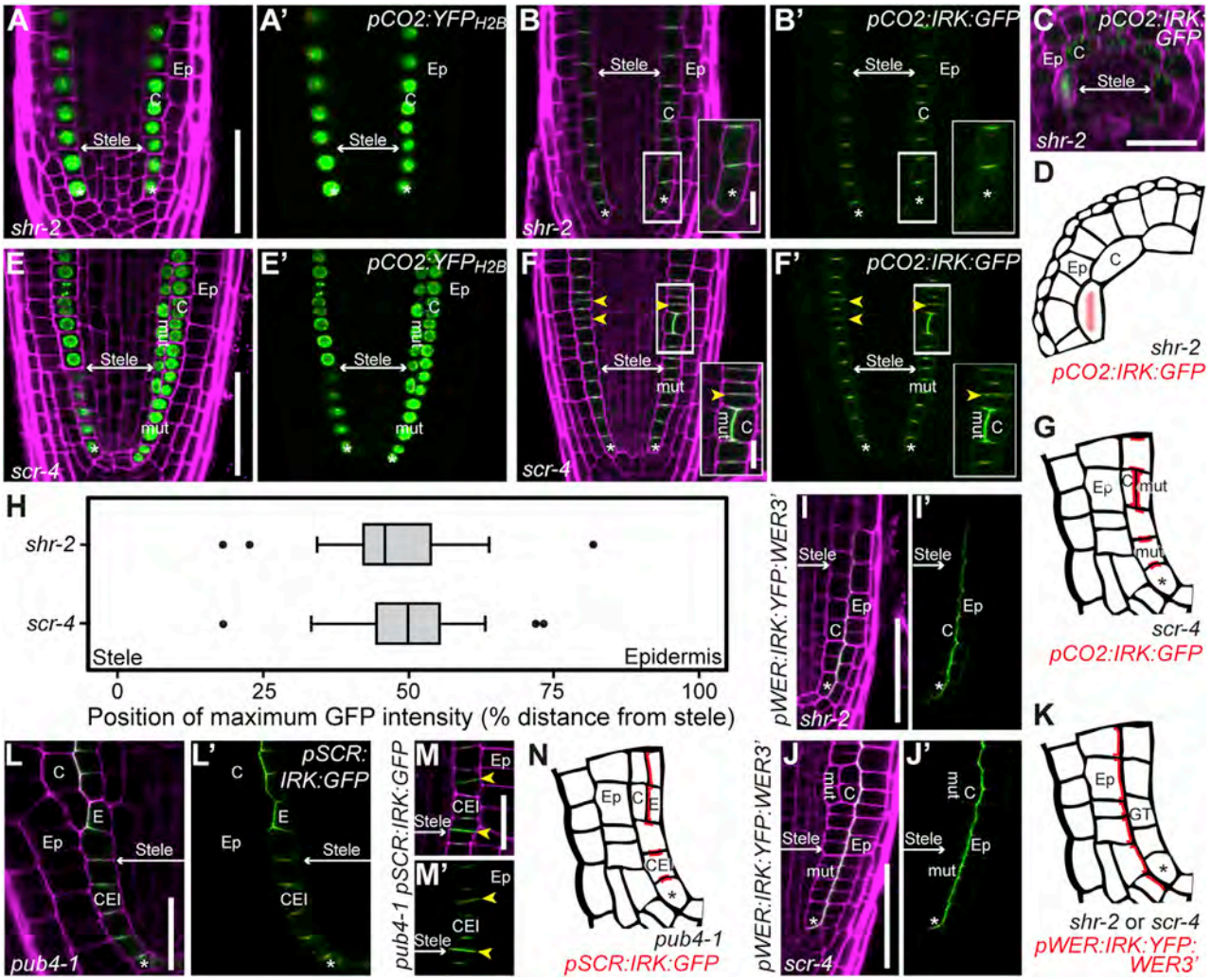

Figure 4. IRK Is Localized to Distinct PM Domains in Ground Tissue Mutants

(A, B, E, F, I, J, and L) Confocal images of roots expressing FPs (green) and stained with PI (magenta). Adjacent panels show PI + FP merged (α) and FP alone (α′). (A) *shr-2* expressing *pCO2:YFP$_{H2B}$* and (B and C) *shr-2* expressing *pCO2:IRK:GFP* (5 dps) and (D) schematic of (C). (E) *scr-4* expressing *pCO2:YFP$_{H2B}$* and (F) *scr-4* expressing *pCO2:IRK:GFP* (7 dps). (G) Schematic of IRK:GFP localization in *scr-4*. (H) Boxplot showing the position of the maximum GFP intensity in single GT layers. Data from a single biological replicate (of three, n = 6 roots per genotype, 5–8 cells per root). Boxes represent the first and third quartiles, median values are marked by the bold line, whiskers indicate 1.5× the interquartile range, and circles indicate outliers. (I and J) *shr-2* and *scr-4* expressing *pWER:IRK:GFP:WER3'* (7 dps). (K) Schematic of IRK-GFP localization in the *shr-2* or *scr-4* epidermis. (L and M) *pub4-1* expressing *pSCR:IRK:GFP* (5 dps). (N) Schematic of IRK-GFP localization in *pub4-1*.

Scale bars: 25 μm in (C), 10 μm in insets of (B) and (F), and 50 μm in all others. Yellow arrowheads in (F) and (M) indicate recently formed PM due to transverse anticlinal cell divisions.

Abbreviations are as follows: C, cortex; mut, mutant layer; Ep, epidermis; CEI, cortex and endodermal initial; E, endodermis; and GT, ground tissue. Asterisks (*) mark GT cells adjacent to the (putative) QC.

(Paquette and Benfey, 2005), our observations are consistent with IRK-GFP accumulation to the inner PM domain of the outermost GT cell layer (likely cortical cell identity) and outer PM domain of the inner GT cell layer (with mutant or mixed cell identity) (Figure 4G). These results indicate that lateral polarity of IRK-GFP occurs only upon formation of two adjacent GT cell layers in *scr*. Additionally, the periclinal cell divisions in *scr* GT appear to align with the centralized localization of IRK-GFP in the rootward and/or shootward PM domains of the single GT layer, thus, IRK-GFP positioning may coincide with the future periclinal cell division plane.

To determine whether altered IRK-GFP localization in *shr* and *scr* was specific to the GT lineage, we examined IRK-GFP localization upon expression from *pWER* in *shr* and *scr.* As in WT, IRK-GFP localized to the inner PM domain of epidermal cells in both *shr* and *scr* mutants (Figures 4I–4K) and was observed whether one or two GT layers were present in *scr*. These results indicate that polar localization of IRK is different from WT only in the *shr* and *scr* single GT layers.

To further explore IRK-GFP localization in roots with single layers of GT, we expressed *pSCR:IRK:GFP* in *pub4* mutants, which have numerous GT initial cells due to delayed periclinal

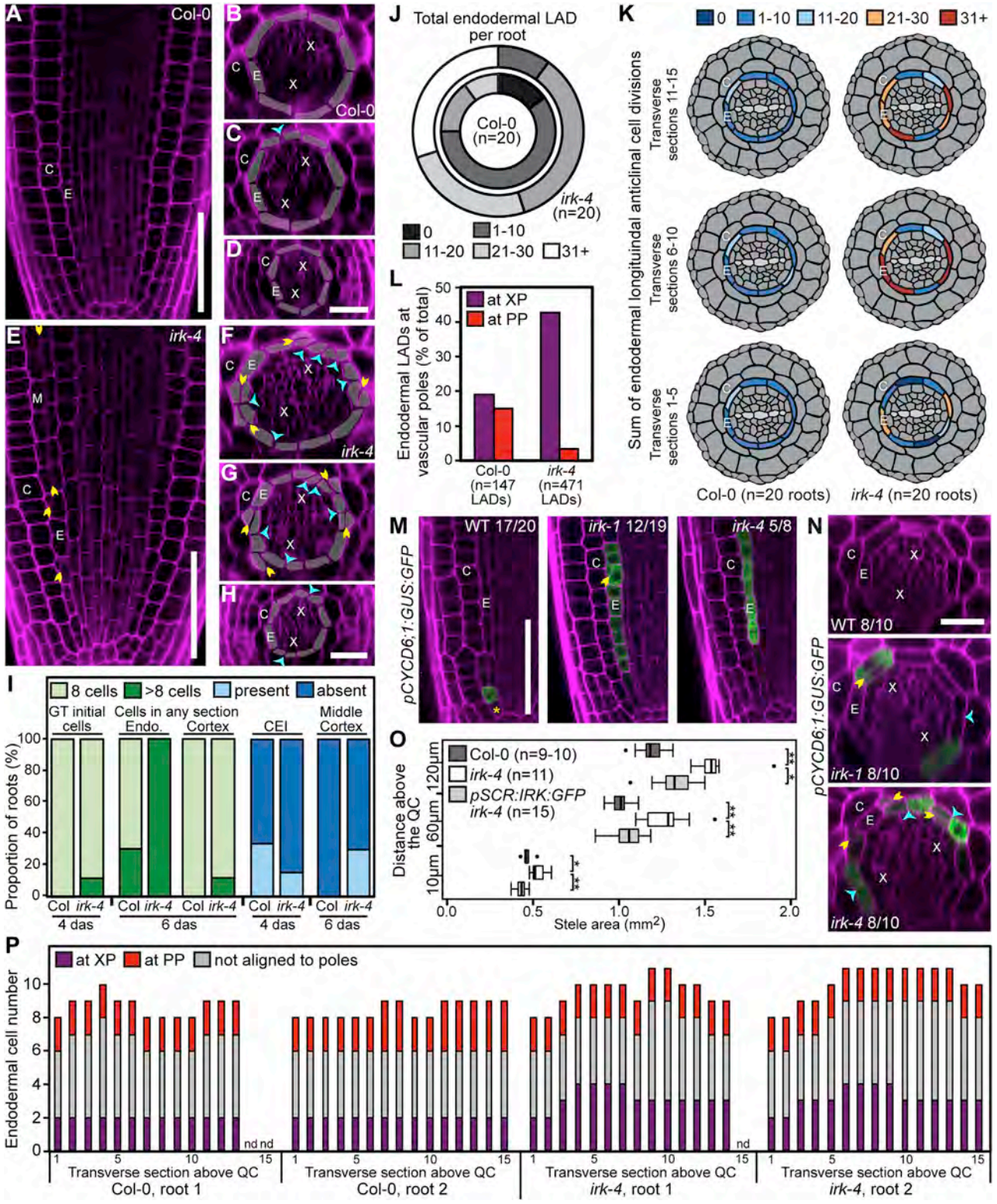

Figure 5. Abnormal Cell Divisions in *irk* Roots Result in GT Cell Proliferation

(A–H) Confocal micrographs of roots at 6 dps stained with PI (magenta). (A and E) Longitudinal root sections, note abnormal timing and orientation of periclinal endodermal cell divisions (yellow arrowheads) in *irk-4*. (B–D and F–H) Transverse sections of roots at (B) and (F) 120 μm, (C) and (G) 60 μm, and (D) and (H) 10 μm above the QC. Note endodermal LADs (cyan arrowheads), endodermal cells, and all daughter cells traced and highlighted to increase visibility.

(legend continued on next page)

Table 1. Quantification of GT Cell Numbers

	Endodermal Cells per Section		Cortex Cells per Section	
	Maximum	Mode	Maximum	Mode
Col-0 (n = 20 roots, 4 dps)	11	8	8	8
irk-4 (n = 22 roots, 4 dps)	14	10	10	8
pSCR:IRK:GFP irk-4 (n = 15 roots, 4 dps)	10	8	8	8
irk-4 (n = 14 roots, 4 dps)	14	10	10	8

See also Figures 5 and S3.

cell division (Kinoshita et al., 2015). In *pub4* mutants, IRK-GFP is localized to the center of the rootward and/or shootward PM domains of CEI and CEID cells (Figures 4L–4N). Additionally, localization of IRK-GFP in the PMs of recent transverse anticlinal cell divisions in *pub4* was more evenly distributed (Figure 4M), further suggesting centralized localization occurs over time. Upon periclinal, formative CEID cell division in *pub4*, IRK-GFP localizes to the outer PM domain in the endodermis (Figures 4L and 4N). Thus, despite cell identity differences between the single GT layers in *scr, shr*, and *pub4*, IRK-GFP localization is similar, accumulating toward the center of the rootward and/or shootward PM domains and becoming localized to a lateral PM domain upon formation of two GT cell layers. Our results indicate that cell identity (an intrinsic cue) is not the primary determinant of IRK localization and instead suggest that IRK-GFP localization is directed by extrinsic cues likely from radially adjacent cells.

Abnormal Cell Divisions in *irk* Roots Result in Irregular GT Organization

Although previous examination of *irk* mutants did not reveal an obvious morphological phenotype (ten Hove et al., 2011; Kanamoto et al., 2002), the specific accumulation pattern of IRK-GFP in the GT suggests that IRK is important for its development. Because changes in IRK-GFP accumulation coincide with formative GT cell divisions, we focused our phenotypic analyses of *irk* mutants on these developmental events. By confocal microscopy, we found that *irk-1* (Salk_038787 (Alonso et al., 2003))exhibited abnormal cell divisions in the GT lineage (Figures S2 and S3A–S3D); however, as the penetrance of this allele is low, we targeted *IRK* for mutagenesis via CRISPR-Cas9 (Fauser et al., 2014) (Figures S2A, S2D, and S2H). We identified two additional *irk* alleles with similar but more severe cell morphology defects and focused further analyses on *irk-4*. Endodermal cells of *irk-4* roots undergo periclinal divisions to form the middle cortex earlier than WT, and occasionally these cell divisions appear misoriented (oblique) (Figures 5A–5H). Additionally, *irk-4* seeds often germinate more quickly than WT (Figure S3M), and *irk-4* GT initial cells undergo premature periclinal division resulting in an absence of persistent CEI (Figure 5I). We occasionally observed disorganization in the *irk-4* stem cell niche consistent with displacement of CEI from the niche and their replacement through division of neighboring initial cells (Figures S3I and S3J). These defects suggest that IRK functions to modulate cell division in the GT lineage.

We also used confocal microscopy to characterize the radial organization of *irk-4* roots by examining serial transverse optical sections from the QC up to 120 μm or 15 cells. While WT roots consistently have 8 GT initial cells, ~15% of *irk-4* roots have >8 GT initial cells. Regardless of cortical or CEI cell number, all *irk-4* roots examined had between 9 and 14 endodermal cells in at least one transverse section. These extra endodermal cells result from LADs (Figures 5A–5K and S3D–S3H; Table 1). While it is consistently reported that WT roots have eight GT cells of any type in the radial axis (Dolan et al., 1993), we find that WT roots occasionally have >8 endodermal cells per section (Table 1; Figures 5J–5L). Our detailed examination revealed that ~30% of Col-0 root tips have no endodermal LADs and most have fewer than a total of 10 per root (Figures 5B–5D and 5J). In contrast, LADs occur more frequently in the *irk-4* endodermis with a majority having >20 per root (Figures 5F–5H, 5J and 5K). Contrary to our expectation, LADs are not propagated in the root's longitudinal axis; therefore, *irk-4* cannot be described as having additional endodermal cell files (Figure 5P; Videos S1 and S2). Furthermore, in *irk*, LADs occur preferentially in endodermal cells aligned with the xylem poles, whereas in Col-0, LADs are more evenly distributed between the vascular axes (Figures 5K, 5L, and S3H). To assess whether *irk* mutants have an increase in all types of GT cell divisions, we examined the number of endodermal and cortical cells in cell files, as a measure of transverse anticlinal cell divisions, and found no substantial difference between WT and *irk-4* (Figure S3N). When comparing *irk* and WT roots (at 4 days post-stratification (dps)), we also observed that the stele area was significantly larger in *irk-4* (Figure 5O). Because endodermal LADs occur frequently at the xylem axis in *irk-4*, we counted the number of xylem cells across the radial axis and found no difference between Col-0 (4.9 cells) and *irk-4* (5.1 cells). To determine whether there was a difference in the width of the xylem or phloem axis in *irk-4*, we measured each axis individually and found that both were increased (Col-0 xylem, 40.6 μm and phloem, 38.2 μm; *irk-4* xylem, 44.7 μm and phloem, 44.7 μm; p-value for phloem width comparison only, < 0.001). This indicates an overall increase in the vascular

(I–L and P) Phenotypic data from one biological replicate (of three, n ≤ 20 roots per genotype, at 4 dps unless otherwise indicated). (I and J) Bar graph and donut plot quantifying phenotypic aspects of *irk-4*. (K) Schematics summarizing endodermal LADs based on position (xylem axis, light gray) and (L) bar graphs showing endodermal LAD frequency at the vascular poles.

(M and N) Confocal images of roots (5 dps) expressing *pCYCD6;1:GUS:GFP* (green) stained with PI (magenta).

(O) Boxplots showing an increased stele area in *irk-4* compared to Col-0 and roots expressing *pSCR:IRK:GFP* (error bars, SD; student's t test, *p < 0.005, **p < 0.0001).

(P) Bar graph showing endodermal cell number, based on position in the radial axis, per transverse section above the QC in two representative roots per genotype (nd, no data).

Abbreviations are as follows: *, CEI; E, endodermis; C, cortex; M, middle cortex; X, xylem axis; XP, xylem pole; and PP, phloem pole.

Scale bars: 50 μm in (A), (E), and (M) and 20 μm in (B)–(D), (F)–(H), and (N).

See also Figures S2 and S3.

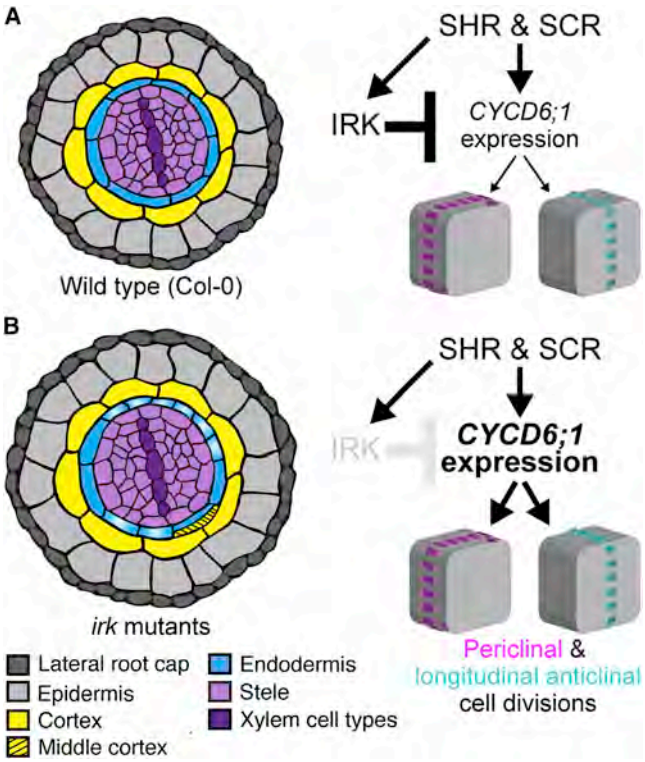

Figure 6. Schematics of WT and *irk* Root Sections and Model for IRK Function

(A) In wild type, SHR and SCR activate *CYCD6;1* expression and SHR putatively activates *IRK* expression (Sozzani et al., 2010). We propose signaling downstream of IRK represses *CYCD6;1* expression and, as a consequence, reduces periclinal and longitudinal anticlinal endodermal cell divisions.

(B) In *irk*, signaling through IRK does not occur; consequently, *CYCD6;1* expression increases along with periclinal and longitudinal anticlinal endodermal cell divisions, which ultimately leads to the increased area of the root's radial axis.

area in *irk* and not a specific increase in the width of the xylem or phloem axis alone.

The abnormal GT cell divisions in *irk* are largely rescued by expression of *pIRK:IRK:GFP* and also by cell layer-specific expression of IRK-GFP (Table 1) from *pSCR*. Additionally, the increased stele area in *irk-4* was rescued by expression of *pSCR:IRK:GFP* (Figure 5O). These results indicate that IRK function in the QC, CEI, CEID, and endodermis is sufficient to largely rescue *irk* root phenotypes and suggest a relationship between GT cell number and stele size in the radial axis. Overall, we find that *irk* mutants have specific defects in GT cell division with early periclinal cell division of the GT stem cells and endodermis and excess endodermal LADs, which collectively extend the GT in the root's radial axis. Together, our data suggest that a signaling pathway involving IRK functions to negatively regulate specific GT cell divisions.

Endodermal LADs Coincide with *pCYCD6;1* Activity

To link IRK function to known regulators of GT cell division, we identified *CYCLIN D6;1* (*CYCD6;1*) as a candidate for misregulation in *irk*. *CYCD6;1* promoter (*pCYCD6;1*) activity occurs during formative cell divisions of GT initial and endodermal cells, and it is not expressed during proliferative (transverse anticlinal) cell divisions (Sozzani et al., 2010). Consistent with previous reports, we observed *pCYCD6;1* activity in endodermal cells in a few WT roots (7 dps), which were starting to form the middle cortex. In contrast, many *irk-1* (7 dps) roots showed *pCYCD6;1* activity along entire files of endodermal cells (Figures S3K and S3L), although middle cortex formation was observed in only ~13% of these roots. Thus, in *irk-1, pCYCD6;1* activity in the endodermis is more extensive than expected for middle cortex formation alone. In younger roots (4–5 dps), *pCYCD6;1* activity is largely restricted to the CEI and CEID in WT, however, in *irk pCYCD6;1*, activity extends shootward in endodermal cell files in the absence of the middle cortex (Figure 5M). In transverse optical sections, we rarely observed *pCYCD6;1* activity above the QC in WT, but in *irk* mutants, *pCYCD6;1* activity co-occurred with endodermal periclinal divisions and LADs (Figure 5N). Thus, *pCYCD6;1* activity outside the stem cell niche coincides with both periclinal and longitudinal anticlinal endodermal cell divisions, suggesting that these cell divisions share a common regulatory mechanism. We propose that signaling downstream of IRK negatively regulates *CYCD6;1* activity to repress endodermal cell divisions in the periclinal and longitudinal anticlinal orientations (Figure 6).

DISCUSSION

Failure to coordinate cell division during development can disrupt organ or tissue function and ultimately impact organism survival. Orchestrating developmental events across tissues requires interpretation of intrinsic and extrinsic cues by individual cells, and polarized (directional) signaling between cell types is implicated in these events. Characterization of IRK provides an important portal to further investigate the links between cell division, cell polarity, and cell-cell communication in root development. Our results indicate that cell polarity and oriented cell division are linked by IRK function in root GT patterning.

With polar localization of IRK-GFP in GT initial and endodermal cells but nonpolar localization in the middle cortex, it is tempting to hypothesize that IRK polarity informs competence for formative cell divisions; however, this hypothesis may be oversimplified. The CEID and endodermis undergo formative periclinal cell divisions; yet, IRK-GFP localizes differently in these cells. Additionally, in the cortex and epidermis, which do not undergo periclinal cell division, IRK-GFP is polarly localized. Therefore, IRK polar accumulation doesn't necessarily coincide with a competence to divide. Nevertheless, IRK functions to negatively regulate specific cell divisions, preventing GT proliferation in the radial axis. IRK may perceive a directional non-cell autonomous cue, perhaps a peptide ligand, which represses these cell divisions. Alternatively, IRK may participate in the recruitment of cell division machinery to the cell division site, specifically during formative cell divisions. These putative roles for IRK are not mutually exclusive and are exciting areas of future investigation.

IRK localization to distinct PM domains in different root cell types is similar to the localization of SCHENGEN1 (SGN1) and SOSEKI1 (SOK1) upon misexpression. *SGN1* encodes a receptor-like cytoplasmic kinase (RLCK) that is required for Casparian strip formation and is localized to the outer PM domain in maturing endodermal cells. Upon misexpression in the root

meristem, SGN1 localizes to the outer PM domain in the endodermis, inner PM domains in the cortex and epidermis, and inner/outer PM domains in the QC (Alassimone et al., 2016). SGN1 is not a transmembrane protein and requires palmitoylation, a post-translational modification, for localization to the PM. SOK1 is also a membrane-associated protein that localizes similar to IRK in the GT and upon misexpression in the root. However, SOK1 is described as edge localized because of its prominent accumulation at the ''corners'' of root cell types and low accumulation at the lateral PM domain in general. This accumulation pattern together with the changes in SOK1 localization in distinct cell types was interpreted to indicate that plant tissues have a universal coordinate system in which spatial information across the different axes are integrated to localize the SOKs (Yoshida et al., 2019). The function of SOK1 or its family members as well as how they physically associate with the PM remain unclear. As membrane-associated proteins, both SGN1 and SOK1 may depend on polarly localized transmembrane proteins such as IRK to serve as interaction partners. The similarity in IRK, SGN1 and SOK1 localization in the root meristem suggests that these proteins localize with respect to the same polarizing cue, which we propose is a locally communicated determinant.

Polar localization of IRK is unique among Arabidopsis transmembrane kinases (LRR-RLKs) and distinct from other laterally polar transmembrane proteins. An Arabidopsis LRR-RLK, SGN3, is considered to be polarly localized as it localizes in a band surrounding maturing endodermal cells; however, outside the endodermis its localization is nonpolar (Alassimone et al., 2016; Pfister et al., 2014). Nutrient transporters, such as BOR1 and NIP5;1, are laterally polar but localize to the same PM domain regardless of cell type. Localization of these transmembrane proteins suggest there are several distinct mechanisms underlying polar protein localization in plant cells. The nutrient transporters are predicted to be oriented by a stele-derived cue (Alassimone et al., 2010), but differential IRK localization among cell types is difficult to reconcile with a global or organ-level polarity determinant. If IRK localization was informed by a global polarity cue, its distinct positioning in adjacent cell types would require a differential readout of the cue in each cell type. Instead, our work is consistent with a hypothesis in which local communication between adjacent cell types informs IRK localization.

Cell identity can be ruled out as the exclusive driver of IRK-GFP localization because its localization in the CEI and CEID of WT and *pub4* and in the single GT layers of *shr* and *scr* is identical, and these cells do not share a common identity. Instead, the common attribute driving IRK localization in these cell types may be the spatial relationships they share. A single layer of GT is bordered by stele and epidermal cell types and IRK-GFP localizes to the center of the rootward and/or shootward domains. When two GT layers are present, each bordered by a GT cell type and another cell type, IRK-GFP is polarized to a lateral PM domain. Additionally, epidermal cells of WT, *shr*, or *scr* are bordered by the lateral root cap and a GT cell type and IRK-GFP localizes to the inner PM domain. We propose that because the spatial relationship between the epidermis and adjacent GT cells in *shr* and *scr* is similar to WT, IRK localization in each genotype is the same. Finally, this ''local cue'' hypothesis can also explain the nonpolar localization of IRK-GFP in the middle or secondary cortex. The middle cortex is a third GT layer bordered exclusively by GT cell types, making it the only cell type bordered by cells of the same tissue in the outer root layers and the only cell type in which IRK-GFP is nonpolar. Together, these observations suggest variable localization of IRK-GFP among different cell types can be tied to information shared locally between neighboring cell types.

Localization of IRK-GFP to the center of the rootward or shootward domains in single GT layers is distinct from the localization of proteins such as CASP1 or SGN3, which localize in a band surrounding differentiating endodermal cells (Roppolo et al., 2011; Pfister et al., 2014). Higher accumulation of polarly localized proteins at the center of the PM domain has been reported for several other proteins including auxin and boron transporters and is attributed to polarized secretion, endosome (re)cycling, and reduced lateral diffusion (Kleine-Vehn et al., 2011; Łangowski et al., 2016). Additionally, polar protein accumulation was shown to depend on the cell wall (Łangowski et al., 2016). Consistent with this, IRK-GFP also appears to be associated with the cell wall. Disentangling whether cell wall removal (protoplasting) results in uniform protein distribution due to disruption of the cell wall specifically or interruption of local cell-cell communication will be a major future challenge. We are intrigued by the centralized accumulation of IRK-GFP in the rootward and shootward domains in single layers of GT, as it aligns with the cell division plane required to form additional GT layers. In *pub4* and *scr*, periclinal cell division resulting in the two GT layers occurs farther from the QC than in WT and thus, this centralized localization precedes cell division in time and space. IRK-GFP is similarly localized in the *shr* single GT layer, suggesting that despite being unable to carry out periclinal cell divisions, *shr* GT cells may establish the correct division plane. Altogether, IRK is implicated in regulation of periclinal cell divisions in the root GT lineage.

Early periclinal GT cell divisions in *irk* root meristems result in few persistent GT initial cells and premature middle cortex formation. Furthermore, numerous LADs in the *irk* endodermis result in excess endodermal cells in the root's radial axis, particularly at the xylem poles. Additionally, LADs are specific to the endodermis and do not occur in neighboring cortex cells. Despite these abnormal GT cell divisions and the enlarged stele area, *irk* roots do not typically exhibit gross morphological or growth defects. Rescue of the GT cell division and stele area defects in *irk* by IRK-GFP expression driven by the *SCR* promoter indicates its expression in the QC, CEI, CEID, and endodermis is sufficient for IRK function and suggests that limiting the endodermal cell number in the radial axis restricts stele area. Endodermal LADs were also observed among serial transverse sections in WT root meristems. These divisions occurred in Col-0 more often than expected based on the literature, however, we most often observed eight endodermal cells surrounding the stele. Similar to *irk*, we found no discernable pattern to these divisions in the WT root's longitudinal axis. Interestingly, specialized endodermal cells, called passage cells, form preferentially at the xylem poles and have no discernable pattern in the root's longitudinal axis (Andersen et al., 2018). Regardless of a possible specialized fate for these endodermal cells upon differentiation in WT or *irk*, our observations indicate that IRK activity represses specific GT cell divisions.

Our observations indicate that meristematic endodermal cells maintain the potential to divide in both the periclinal and longitudinal anticlinal orientations and that the occurrence of these cell divisions is impinged upon by IRK activity. *pCYCD6;1* activity is associated with formative cell divisions in the GT lineage (Sozzani et al., 2010), and expression of specific D-type CYCLINs has been linked to other formative cell divisions in plant development (Han et al., 2018; Kono et al., 2007; Weimer et al., 2018). In *irk* mutants, *pCYCD6;1* is highly active and associated not only with GT formative cell divisions but with endodermal LADs. We propose that CYCD6;1 activity in the endodermis is downstream of IRK-mediated signal transduction. Intriguingly, *CYCD6;1* is a known direct target of SHR and *IRK* is a putative SHR direct target (Sozzani et al., 2010), suggesting that SHR activity both positively and negatively influences specific GT cell divisions (Figure 6). Our results suggest that periclinal and longitudinal anticlinal GT cell divisions have shared regulatory circuitry and that endodermal LADs are developmentally regulated.

Conclusions

Our results are consistent with the presence of an intercellular signaling mechanism operating in the root's radial axis and outside the stem cell niche to repress specific cell divisions and inform protein localization. Polar localization of IRK and its role in restricting GT cell divisions lead naturally to the hypothesis that IRK perceives a repressive cue from peripheral (outer) cell layers. The identity of this extrinsic cue as well as the downstream events in IRK-mediated signaling remain unknown. We propose that differential IRK localization across root cell types is driven by local, positional information from adjacent cells. This proposed mechanism for IRK localization supports the long-standing hypothesis that positional information is a key driver of root development and, more broadly, suggests that perception of directional cues may occur via polarized transmembrane receptor kinases. Polar localization of a subset of RLKs may facilitate heterodimeric interactions between LRR-RLKs that function in specific signaling events. Ultimately, partitioning the PM into distinct signaling domains presents a straightforward mechanism to achieve specificity in LRR-RLK-mediated signaling and/or provide membrane-anchored scaffolds that recruit protein complexes required for oriented, intracellular processes.

STAR★METHODS

Detailed methods are provided in the online version of this paper and include the following:

- KEY RESOURCES TABLE
- LEAD CONTACT AND MATERIALS AVAILABILITY
- EXPERIMENTAL MODEL AND SUBJECT DETAILS
- METHODS DETAILS
  - Vector Construction and Plant Transformation
  - Confocal Microscopy and Image Analysis
  - Plasmolysis and Cell Wall Degradation Treatments
  - Phenotypic Analyses
  - RT-qPCR Analysis
- QUANTIFICATION AND STATISTICAL ANALYSIS
- DATA AND CODE AVAILABILITY

SUPPLEMENTAL INFORMATION

Supplemental Information can be found online at https://doi.org/10.1016/j.devcel.2019.12.001.

ACKNOWLEDGMENTS

We thank Dr. Carolyn Rasmussen (UCR), Ross Sozzani (NCSU), and Philip Benfey (Duke University) for reading drafts and providing comments on this manuscript while it was in preparation. We thank Dr. Philip Benfey and Dr. Jingyuan Zhang (Duke University) for gracious sharing of molecular biology and plant reagents and resources. We thank Jeff Long (UCLA) for sharing reagents and expertise in embryonic expression and localization analyses. We appreciate access to and microscopy assistance from the Institute of Integrative Genome Biology Microscopy Core Faculty (UC Riverside) and David Carter. We are grateful to the anonymous reviewers for their thoughtful and constructive comments on this manuscript and for their quick turnaround time. This work was supported by Initial Compliment (IC) funds from the University of California, Riverside, USDA-NIFA-CA-R-BPS-5156-H and NSF CAREER award #1751385 to J.M.V.N.

AUTHOR CONTRIBUTIONS

Conceptualization, J.M.V.N.; Methodology and Investigation, J.M.V.N., R.C., J.G., and C.R.-F.; Resources, J.M.V.N. and R.C.; Writing – Original Draft: J.M.V.N.; Writing – Review and Editing, J.M.V.N., R.C., J.G., and C.R.-F.; Visualization, J.M.V.N., R.C., J.G., and C.R.-F.; Supervision and Funding Acquisition, J.M.V.N.

DECLARATION OF INTERESTS

The authors declare no competing interests.

Received: May 24, 2019
Revised: September 30, 2019
Accepted: November 25, 2019
Published: December 26, 2019

REFERENCES

Alassimone, J., Fujita, S., Doblas, V.G., van Dop, M., Barberon, M., Kalmbach, L., Vermeer, J.E., Rojas-Murcia, N., Santuari, L., Hardtke, C.S., and Geldner, N. (2016). Polarly localized kinase SGN1 is required for Casparian strip integrity and positioning. Nat. Plants *2*, 16113.

Alassimone, J., Naseer, S., and Geldner, N. (2010). A developmental framework for endodermal differentiation and polarity. Proc. Natl. Acad. Sci. USA *107*, 5214–5219.

Alonso, J.M., Stepanova, A.N., Leisse, T.J., Kim, C.J., Chen, H., Shinn, P., Stevenson, D.K., Zimmerman, J., Barajas, P., Cheuk, R., et al. (2003). Genome-wide insertional mutagenesis of Arabidopsis thaliana. Science *301*, 653–657.

Andersen, T.G., Naseer, S., Ursache, R., Wybouw, B., Smet, W., De Rybel, B., Vermeer, J.E.M., and Geldner, N. (2018). Diffusible repression of cytokinin signalling produces endodermal symmetry and passage cells. Nature *555*, 529–533.

Barberon, M., Dubeaux, G., Kolb, C., Isono, E., Zelazny, E., and Vert, G. (2014). Polarization of IRON-REGULATED TRANSPORTER 1 (IRT1) to the plant-soil interface plays crucial role in metal homeostasis. Proc. Natl. Acad. Sci. USA *111*, 8293–8298.

Baum, S.F., Dubrovsky, J.G., and Rost, T.L. (2002). Apical organization and maturation of the cortex and vascular cylinder in Arabidopsis thaliana (Brassicaceae) roots. Am. J. Bot. *89*, 908–920.

Benfey, P.N., Linstead, P.J., Roberts, K., Schiefelbein, J.W., Hauser, M.T., and Aeschbacher, R.A. (1993). Root development in Arabidopsis: four mutants with dramatically altered root morphogenesis. Development *119*, 57–70.

Birnbaum, K., Shasha, D.E., Wang, J.Y., Jung, J.W., Lambert, G.M., Galbraith, D.W., and Benfey, P.N. (2003). A gene expression map of the Arabidopsis root. Science *302*, 1956–1960.

Brady, S.M., Orlando, D.A., Lee, J.Y., Wang, J.Y., Koch, J., Dinneny, J.R., Mace, D., Ohler, U., and Benfey, P.N. (2007). A high-resolution root spatiotemporal map reveals dominant expression patterns. Science *318*, 801–806.

Breda, A.S., Hazak, O., and Hardtke, C.S. (2017). Phosphosite charge rather than shootward localization determines OCTOPUS activity in root protophloem. Proc. Natl. Acad. Sci. USA *114*, E5721–E5730.

Carlsbecker, A., Lee, J.Y., Roberts, C.J., Dettmer, J., Lehesranta, S., Zhou, J., Lindgren, O., Moreno-Risueno, M.A., Vatén, A., Thitamadee, S., et al. (2010). Cell signalling by microRNA165/6 directs gene dose-dependent root cell fate. Nature *465*, 316–321.

Cartwright, H.N., Humphries, J.A., and Smith, L.G. (2009). PAN1: a receptor-like protein that promotes polarization of an asymmetric cell division in maize. Science *323*, 649–651.

Clough, S.J., and Bent, A.F. (1998). Floral dip: a simplified method for Agrobacterium-mediated transformation of Arabidopsis thaliana. Plant J. *16*, 735–743.

Crawford, B.C.W., Sewell, J., Golembeski, G., Roshan, C., Long, J.A., and Yanofsky, M.F. (2015). Plant development. Genetic control of distal stem cell fate within root and embryonic meristems. Science *347*, 655–659.

Czechowski, T., Stitt, M., Altmann, T., Udvardi, M.K., and Scheible, W.R. (2005). Genome-wide identification and testing of superior reference genes for transcript normalization in Arabidopsis. Plant Physiol. *139*, 5–17.

Depuydt, S., Rodriguez-Villalon, A., Santuari, L., Wyser-Rmili, C., Ragni, L., and Hardtke, C.S. (2013). Suppression of Arabidopsis protophloem differentiation and root meristem growth by CLE45 requires the receptor-like kinase BAM3. Proc. Natl. Acad. Sci. USA *110*, 7074–7079.

Di Laurenzio, L., Wysocka-Diller, J., Malamy, J.E., Pysh, L., Helariutta, Y., Freshour, G., Hahn, M.G., Feldmann, K.A., and Benfey, P.N. (1996). The SCARECROW gene regulates an asymmetric cell division that is essential for generating the radial organization of the Arabidopsis root. Cell *86*, 423–433.

Doblas, V.G., Smakowska-Luzan, E., Fujita, S., Alassimone, J., Barberon, M., Madalinski, M., Belkhadir, Y., and Geldner, N. (2017). Root diffusion barrier control by a vasculature-derived peptide binding to the SGN3 receptor. Science *355*, 280–284.

Dolan, L., Janmaat, K., Willemsen, V., Linstead, P., Poethig, S., Roberts, K., and Scheres, B. (1993). Cellular organisation of the Arabidopsis thaliana root. Development *119*, 71–84.

Dong, J., MacAlister, C.A., and Bergmann, D.C. (2009). BASL controls asymmetric cell division in Arabidopsis. Cell *137*, 1320–1330.

Etchells, J.P., Smit, M.E., Gaudinier, A., Williams, C.J., and Brady, S.M. (2016). A brief history of the TDIF-PXY signalling module: balancing meristem identity and differentiation during vascular development. New Phytol. *209*, 474–484.

Etchells, J.P., and Turner, S.R. (2010). The PXY-CLE41 receptor ligand pair defines a multifunctional pathway that controls the rate and orientation of vascular cell division. Development *137*, 767–774.

Facette, M.R., Park, Y., Sutimantanapi, D., Luo, A., Cartwright, H.N., Yang, B., Bennett, E.J., Sylvester, A.W., and Smith, L.G. (2015). The SCAR/WAVE complex polarizes PAN receptors and promotes division asymmetry in maize. Nat. Plants *1*, 14024.

Facette, M.R., Rasmussen, C.G., and Van Norman, J.M. (2019). A plane choice: coordinating timing and orientation of cell division during plant development. Curr. Opin. Plant Biol. *47*, 47–55.

Fauser, F., Schiml, S., and Puchta, H. (2014). Both CRISPR/Cas-based nucleases and nickases can be used efficiently for genome engineering in Arabidopsis thaliana. Plant J. *79*, 348–359.

Feraru, E., Feraru, M.I., Kleine-Vehn, J., Martinière, A., Mouille, G., Vanneste, S., Vernhettes, S., Runions, J., and Friml, J. (2011). PIN polarity maintenance by the cell wall in Arabidopsis. Curr. Biol. *21*, 338–343.

Gallagher, K.L., Paquette, A.J., Nakajima, K., and Benfey, P.N. (2004). Mechanisms regulating SHORT-ROOT intercellular movement. Curr. Biol. *14*, 1847–1851.

Han, S.K., Qi, X., Sugihara, K., Dang, J.H., Endo, T.A., Miller, K.L., Kim, E.D., Miura, T., and Torii, K.U. (2018). MUTE directly orchestrates cell-state switch and the single symmetric division to create stomata. Dev. Cell *45*, 303–315.e5.

Heidstra, R., Welch, D., and Scheres, B. (2004). Mosaic analyses using marked activation and deletion clones dissect Arabidopsis SCARECROW action in asymmetric cell division. Genes Dev. *18*, 1964–1969.

Helariutta, Y., Fukaki, H., Wysocka-Diller, J., Nakajima, K., Jung, J., Sena, G., Hauser, M.T., and Benfey, P.N. (2000). The SHORT-ROOT gene controls radial patterning of the Arabidopsis root through radial signaling. Cell *101*, 555–567.

Hirakawa, Y., Shinohara, H., Kondo, Y., Inoue, A., Nakanomyo, I., Ogawa, M., Sawa, S., Ohashi-Ito, K., Matsubayashi, Y., and Fukuda, H. (2008). Non-cell-autonomous control of vascular stem cell fate by a CLE peptide/receptor system. Proc. Natl. Acad. Sci. USA *105*, 15208–15213.

Kanamoto, H., Hattan, J., Takemura, M., Yokota, A., and Kohchi, T. (2002). Molecular cloning and characterization of a gene coding for a putative receptor-like protein kinase with a leucine-rich repeat expressed in inflorescence and root apices from Arabidopsis. Plant Biotechnol. *19*, 113–120.

Kidner, C., Sundaresan, V., Roberts, K., and Dolan, L. (2000). Clonal analysis of the Arabidopsis root con®rms that position, not lineage, determines cell fate. Planta *21*, 191–199.

Kinoshita, A., ten Hove, C.A., Tabata, R., Yamada, M., Shimizu, N., Ishida, T., Yamaguchi, K., Shigenobu, S., Takebayashi, Y., Iuchi, S., et al. (2015). A plant U-box protein, PUB4, regulates asymmetric cell division and cell proliferation in the root meristem. Development *142*, 444–453.

Kleine-Vehn, J., Wabnik, K., Martinière, A., Łangowski, Ł., Willig, K., Naramoto, S., Leitner, J., Tanaka, H., Jakobs, S., Robert, S., et al. (2011). Recycling, clustering, and endocytosis jointly maintain PIN auxin carrier polarity at the plasma membrane. Mol. Syst. Biol. *7*, 540.

Koizumi, K., Hayashi, T., Wu, S., and Gallagher, K.L. (2012). The SHORT-ROOT protein acts as a mobile, dose-dependent signal in patterning the ground tissue. Proc. Natl. Acad. Sci. USA *109*, 13010–13015.

Koncz, C., Németh, K., Rédei, G.P., and Schell, J. (1992). T-DNA insertional mutagenesis in Arabidopsis. Plant Mol. Biol. *20*, 963–976.

Kono, A., Umeda-Hara, C., Adachi, S., Nagata, N., Konomi, M., Nakagawa, T., Uchimiya, H., and Umeda, M. (2007). The Arabidopsis D-type cyclin CYCD4 controls cell division in the stomatal lineage of the hypocotyl epidermis. Plant Cell *19*, 1265–1277.

Łangowski, Ł., Wabnik, K., Li, H., Vanneste, S., Naramoto, S., Tanaka, H., and Friml, J. (2016). Cellular mechanisms for cargo delivery and polarity maintenance at different polar domains in plant cells. Cell Discov. *2*, 16018.

Lau, O.S., and Bergmann, D.C. (2012). Stomatal development: a plant's perspective on cell polarity, cell fate transitions and intercellular communication. Development *139*, 3683–3692.

Lee, J.Y., Colinas, J., Wang, J.Y., Mace, D., Ohler, U., and Benfey, P.N. (2006). Transcriptional and posttranscriptional regulation of transcription factor expression in Arabidopsis roots. Proc. Natl. Acad. Sci. USA *103*, 6055–6060.

Lee, M.M., and Schiefelbein, J. (1999). Werewolf, a MYB-related protein in Arabidopsis, is a position-dependent regulator of epidermal cell patterning. Cell *99*, 473–483.

Levesque, M.P., Vernoux, T., Busch, W., Cui, H., Wang, J.Y., Blilou, I., Hassan, H., Nakajima, K., Matsumoto, N., Lohmann, J.U., et al. (2006). Whole-genome analysis of the SHORT-ROOT developmental pathway in Arabidopsis. PLoS Biol. *4*, e143.

Li, S., Yamada, M., Han, X., Ohler, U., and Benfey, P.N. (2016). High-resolution expression map of the Arabidopsis Root reveals alternative splicing and lincRNA regulation. Dev. Cell *39*, 508–522.

Ma, J.F., Tamai, K., Yamaji, N., Mitani, N., Konishi, S., Katsuhara, M., Ishiguro, M., Murata, Y., and Yano, M. (2006). A silicon transporter in rice. Nature *440*, 688–691.

Ma, J.F., Yamaji, N., Mitani, N., Tamai, K., Konishi, S., Fujiwara, T., Katsuhara, M., and Yano, M. (2007). An efflux transporter of silicon in rice. Nature *448*, 209–212.

Marhava, P., Hoermayer, L., Yoshida, S., Marhavý, P., Benková, E., and Friml, J. (2019). Re-activation of stem cell pathways for pattern restoration in plant wound healing. Cell *177*, 957–969.e13.

Miyashima, S., Koi, S., Hashimoto, T., and Nakajima, K. (2011). Non-cell-autonomous microRNA165 acts in a dose-dependent manner to regulate multiple differentiation status in the Arabidopsis root. Development *138*, 2303–2313.

Morita, J., Kato, K., Nakane, T., Kondo, Y., Fukuda, H., Nishimasu, H., Ishitani, R., and Nureki, O. (2016). Crystal structure of the plant receptor-like kinase TDR in complex with the TDIF peptide. Nat. Commun. *7*, 12383.

Nakajima, K., and Benfey, P.N. (2002). Signaling in and out: control of cell division and differentiation in the shoot and root. Plant Cell *14*, S265–S276.

Nakajima, K., Sena, G., Nawy, T., and Benfey, P.N. (2001). Intercellular movement of the putative transcription factor SHR in root patterning. Nature *413*, 307–311.

Nakamura, M., and Grebe, M. (2018). Outer, inner and planar polarity in the Arabidopsis root. Curr. Opin. Plant Biol. *41*, 46–53.

Okuda, S., Fujita, S., Moretti, A., Hohmann, U., Doblas, V.G., Ma, Y., Pfister, A., Brandt, B., Geldner, N., and Hothorn, M. (2019). Molecular mechanism for the recognition of sequence-divergent CIF peptides by the plant receptor kinases GSO1/SGN3 and GSO2. bioRxiv. https://doi.org/10.1101/692228.

Paquette, A.J., and Benfey, P.N. (2005). Maturation of the ground tissue of the root is regulated by gibberellin and SCARECROW and requires SHORTROOT. Plant Physiol. *138*, 636–640.

Petrásek, J., and Friml, J. (2009). Auxin transport routes in plant development. Development *136*, 2675–2688.

Pfister, A., Barberon, M., Alassimone, J., Kalmbach, L., Lee, Y., Vermeer, J.E., Yamazaki, M., Li, G., Maurel, C., Takano, J., et al. (2014). A receptor-like kinase mutant with absent endodermal diffusion barrier displays selective nutrient homeostasis defects. eLife *3*, e03115.

Pillitteri, L.J., Peterson, K.M., Horst, R.J., and Torii, K.U. (2011). Molecular profiling of stomatal Meristemoids reveals new component of asymmetric cell division and commonalities among stem cell populations in Arabidopsis. Plant Cell *23*, 3260–3275.

Qian, P., Song, W., Yokoo, T., Minobe, A., Wang, G., Ishida, T., Sawa, S., Chai, J., and Kakimoto, T. (2018). The CLE9/10 secretory peptide regulates stomatal and vascular development through distinct receptors. Nat. Plants *4*, 1071–1081.

Rasmussen, C.G., and Bellinger, M. (2018). An overview of plant division-plane orientation. New Phytol. *219*, 505–512.

Roppolo, D., De Rybel, B., Dénervaud Tendon, V., Pfister, A., Alassimone, J., Vermeer, J.E., Yamazaki, M., Stierhof, Y.D., Beeckman, T., and Geldner, N. (2011). A novel protein family mediates Casparian strip formation in the endodermis. Nature *473*, 380–383.

Rowe, M.H., Dong, J., Weimer, A.K., and Bergmann, D.C. (2019). A plant-specific polarity module establishes cell fate asymmetry in the Arabidopsis stomatal lineage. bioRxiv https://www.biorxiv.org/content/10.1101/614636v1.

Scacchi, E., Osmont, K.S., Beuchat, J., Salinas, P., Navarrete-Gómez, M., Trigueros, M., Ferrándiz, C., and Hardtke, C.S. (2009). Dynamic, auxin-responsive plasma membrane-to-nucleus movement of Arabidopsis BRX. Development *136*, 2059–2067.

Scheres, B., Di Laurenzio, L., Willemsen, V., Hauser, M.T., Janmaat, K., Weisbeek, P., and Benfey, P.N. (1995). Mutations affecting the radial organisation of the Arabidopsis root display specific defects throughout the embryonic axis. Development *121*, 53–62.

Scheres, B., and Benfey, P.N. (1999). Asymmetric cell division in plants. Annu. Rev. Plant Physiol. Plant Mol. Biol. *50*, 505–537.

Shao, W., and Dong, J. (2016). Polarity in plant asymmetric cell division: division orientation and cell fate differentiation. Dev. Biol. *419*, 121–131.

Shi, C.L., von Wangenheim, D., Herrmann, U., Wildhagen, M., Kulik, I., Kopf, A., Ishida, T., Olsson, V., Anker, M.K., Albert, M., et al. (2018). The dynamics of root cap sloughing in Arabidopsis is regulated by peptide signalling. Nat. Plants *4*, 596–604.

Shiu, S.H., and Bleecker, A.B. (2001). Receptor-like kinases from Arabidopsis form a monophyletic gene family related to animal receptor kinases. Proc. Natl. Acad. Sci. USA *98*, 10763–10768.

Shiu, S.H., and Bleecker, A.B. (2003). Expansion of the receptor-like kinase/Pelle gene family and receptor-like proteins in Arabidopsis. Plant Physiol. *132*, 530–543.

Sozzani, R., Cui, H., Moreno-Risueno, M.A., Busch, W., Van Norman, J.M., Vernoux, T., Brady, S.M., Dewitte, W., Murray, J.A., and Benfey, P.N. (2010). Spatiotemporal regulation of cell-cycle genes by SHORTROOT links patterning and growth. Nature *466*, 128–132.

Takano, J., Tanaka, M., Toyoda, A., Miwa, K., Kasai, K., Fuji, K., Onouchi, H., Naito, S., and Fujiwara, T. (2010). Polar localization and degradation of Arabidopsis boron transporters through distinct trafficking pathways. Proc. Natl. Acad. Sci. USA *107*, 5220–5225.

ten Hove, C.A., Bochdanovits, Z., Jansweijer, V.M., Koning, F.G., Berke, L., Sanchez-Perez, G.F., Scheres, B., and Heidstra, R. (2011). Probing the roles of LRR RLK genes in Arabidopsis thaliana roots using a custom T-DNA insertion set. Plant Mol. Biol. *76*, 69–83.

Truernit, E., Bauby, H., Belcram, K., Barthélémy, J., and Palauqui, J.C. (2012). OCTOPUS, a polarly localised membrane-associated protein, regulates phloem differentiation entry in Arabidopsis thaliana. Development *139*, 1306–1315.

van den Berg, C., Willemsen, V., Hage, W., Weisbeek, P., and Scheres, B. (1995). Cell fate in the Arabidopsis root meristem determined by directional signalling. Nature *378*, 62–65.

van den Berg, C., Willemsen, V., Hendriks, G., Weisbeek, P., and Scheres, B. (1997). Short-range control of cell differentiation in the Arabidopsis root meristem. Nature *390*, 287–289.

Van Norman, J.M. (2016). Asymmetry and cell polarity in root development. Dev. Biol. *419*, 165–174.

Van Norman, J.M., Breakfield, N.W., and Benfey, P.N. (2011). Intercellular communication during plant development. Plant Cell *23*, 855–864.

Van Norman, J.M., Zhang, J., Cazzonelli, C.I., Pogson, B.J., Harrison, P.J., Bugg, T.D., Chan, K.X., Thompson, A.J., and Benfey, P.N. (2014). Periodic root branching in Arabidopsis requires synthesis of an uncharacterized carotenoid derivative. Proc. Natl. Acad. Sci. USA *111*, E1300–E1309.

Weimer, A.K., Matos, J.L., Sharma, N., Patell, F., Murray, J.A.H., Dewitte, W., and Bergmann, D.C. (2018). Lineage- and stage-specific expressedCYCD7; 1coordinates the single symmetric division that creates stomatal guard cells. Development *145*, dev160671.

Wisniewska, J., Xu, J., Seifertová, D., Brewer, P.B., Ruzicka, K., Blilou, I., Rouquié, D., Benková, E., Scheres, B., and Friml, J. (2006). Polar PIN localization directs auxin flow in plants. Science *312*, 883.

Wysocka-Diller, J.W., Helariutta, Y., Fukaki, H., Malamy, J.E., and Benfey, P.N. (2000). Molecular analysis of SCARECROW function reveals a radial patterning mechanism common to root and shoot. Development *127*, 595–603.

Yoshida, S., van der Schuren, A., van Dop, M., van Galen, L., Saiga, S., Adibi, M., Möller, B., Ten Hove, C.A., Marhavy, P., Smith, R., et al. (2019). A SOSEKI-based coordinate system interprets global polarity cues in Arabidopsis. Nat. Plants *5*, 160–166.

Zhang, X., Facette, M., Humphries, J.A., Shen, Z., Park, Y., Sutimantanapi, D., Sylvester, A.W., Briggs, S.P., and Smith, L.G. (2012). Identification of PAN2 by quantitative proteomics as a leucine-rich repeat-receptor-like kinase acting upstream of PAN1 to polarize cell division in maize. Plant Cell *24*, 4577–4589.

STAR★METHODS

KEY RESOURCES TABLE

REAGENT or RESOURCE	SOURCE	IDENTIFIER
Bacterial and Virus Strains		
Agrobacterium GV3101	(Koncz et al., 1992)	N/A
Chemicals, Peptides, and Recombinant Proteins		
RNeasy Plant mini kit	Qiagen	Cat#74904
RevertAid First Strand cDNA Synthesis Kit	Thermo Scientific	Cat#K1622
IQ SYBR Green Supermix	Bio Rad	Cat#1708882
Experimental Models: Organisms/Strains		
Col-0, *pIRK:erGFP*	This paper, plant transformation	N/A
Col-0, *pIRK:IRK:GFP*	This paper, plant transformation	N/A
Col-0, *pSCR:IRK:GFP*	This paper, plant transformation	N/A
irk-4	This paper, CRISPR-Cas9 induced	N/A
irk-4, *pIRK:IRK:GFP*	This paper, genetic cross	N/A
irk-1 (Salk_038787)	(Alonso et al., 2003)	N/A
irk-1, *pIRK:IRK:GFP*	This paper, genetic cross	N/A
irk-4, *pSCR:IRK:GFP*	This paper, genetic cross	N/A
Col-0, *pCO_2:IRK:GFP*	This paper, plant transformation	N/A
Col-0, *pWER:IRK:YFP:WER3'*	This paper, plant transformation	N/A
Col-0, *pWER:erGFP:WER3'*	This paper, plant transformation	N/A
Col-0, *pCYCD6;1:GUS:GFP*	(Sozzani et al., 2010)	N/A
irk-4, *pCYCD6;1:GUS:GFP*	This paper, genetic cross	N/A
irk-1, *pCYCD6;1:GUS:GFP*	This paper, genetic cross	N/A
scr-4	(Di Laurenzio et al., 1996; Wysocka-Diller et al., 2000)	N/A
scr-4, *pCO_2:IRK:GFP*	This paper, genetic cross	N/A
shr-2	(Helariutta et al., 2000)	N/A
shr-2, *pCO_2:IRK:GFP*	This paper, genetic cross	N/A
scr-4, *pWER:IRK:YFP:WER3'*	This paper, genetic cross	N/A
shr-2, *pWER:IRK:YFP:WER3'*	This paper, genetic cross	N/A
pub4-1, *pSCR:IRK:GFP*	This paper, genetic cross	N/A
pub4-1 (Salk_108269)	(Kinoshita et al., 2015)	N/A
Oligonucleotides		
Genotyping primers	Table S1, this paper	N/A
Cloning primers	Table S1, this paper	N/A
qRT-PCR primers	Table S2, this paper	N/A
Recombinant DNA		
pIRK:erGFP	This paper	N/A
pIRK:IRK:GFP	This paper	N/A
pSCR:IRK:GFP	This paper	N/A
pCO_2:IRK:GFP	This paper	N/A
pWER:IRK:YFP:WER3'	This paper	N/A
Software and Algorithms		
A plasmid editor (ApE)	M. Wayne Davis, http://jorgensen.biology.utah.edu/wayned/ape/	N/A
LAS X	Leica Microsystems, https://www.leica-microsystems.com/products/microscope-software/p/leica-las-x-ls/	N/A
Zen, Black Edition	Zeiss Microscopy, https://www.zeiss.com/microscopy/int/products/microscope-software/zen-lite.html	N/A

(*Continued on next page*)

Continued

REAGENT or RESOURCE	SOURCE	IDENTIFIER
ImageJ	NIH, https://imagej.nih.gov/ij/	N/A
Photoshop and Illustrator	Adobe, http://www.adobe.com	N/A
Excel	Microsoft	N/A
R version 3.4.0	The R Project for Statistical Computing, https://www.r-project.org	
Imaris x64 9.1.2 software	Bitplane, Oxford Instruments, https://imaris.oxinst.com/	N/A

LEAD CONTACT AND MATERIALS AVAILABILITY

Further information and requests for resources and reagents should be directed to and will be fulfilled by the Lead Contact, Jaimie Van Norman (jaimie.vannorman@ucr.edu). Plasmids and transgenic Arabidopsis lines generated in this study have been deposited to the Arabidopsis Resource Center (ABRC, https://abrc.osu.edu/).

EXPERIMENTAL MODEL AND SUBJECT DETAILS

The *Arabidopsis thaliana* Columbia-0 accession was used as wild type, unless otherwise indicated. Seeds were surface sterilized with chlorine gas and plated on 1% MS agar media in 100 milliimeter square Petri plates. Standard growth medium consisted of 1× Murashige and Skoog salts (Caisson labs), 0.5g/L MES (EMD), 1% sucrose, pH 5.7, and 1% agar (Difco). The seeds were sown on plates and stratified on growth medium at 4°C for 2–3 days and subsequently placed vertically in a Percival incubator and under long day conditions (16 h light/8 h dark) at a constant temperature of 22°C. Plates were typically sealed with parafilm for experimental analyses. Seedlings grown on plates sealed with 3M micropore tape were examined for mutant phenotypes and IRK-GFP localization and no substantial differences were observed. Seedlings were typically examined between 4-7 days post-stratification (dps), unless otherwise noted and details for individual experiments are listed in figure legends and/or below.

Candidate alleles of *IRK* were obtained from the ABRC (Arabidopsis Resource Center): Salk_038787 (*irk-1*), Salk_045838 (*irk-2*) and Salk_079802 (*irk-3*) (Alonso et al., 2003). The *pub4-1* allele was ordered from the ABRC (Salk_108269 (Kinoshita et al., 2015)) and the *shr-2* and *scr-4* alleles (Helariutta et al., 2000; Di Laurenzio et al., 1996; Wysocka-Diller et al., 2000) were provided by Philip Benfey (Duke University, Durham, NC, USA). PCR-based assays were used to genotype all T-DNA alleles and the primers utilized in this study are listed in Table S1. The cell type-specific reporters pCO_2*:YFP*$_{H2B}$ (Heidstra et al., 2004), *pSCR:erGFP* ((Wysocka-Diller et al., 2000; Levesque et al., 2006)), and *pCYCD6;1:GUS:GFP* (Sozzani et al., 2010) were also received from the Benfey lab. Crosses between *irk* alleles and various reporters were done by standard methods. Two independent lines expressing *pCYCD6;1:GUS:GFP* were examined and crossed to *irk* with no detectable difference in their expression either in wild type or *irk*. Two representative, independent lines expressing pCO_2*:IRK:GFP* were crossed with *shr-2* and *scr-4* heterozygous plants. Plants homozygous for pCO_2*:IRK*:*GFP* and heterozygous for either *shr-2* or *scr-4* were chosen for subsequent analyses and no differences between the independent reporter lines were observed in the *shr* and *scr* backgrounds. Confocal images of IRK-GFP localization were obtained for *shr-2* and *scr-4* at 5 and 7 dps, respectively. Two representative, independent lines expressing *pSCR:IRK:GFP* were crossed with *pub4-1* homozygous mutant plants. Plants homozygous for *pSCR:IRK:GFP* and *pub4-1* were chosen for subsequent analyses and no differences between the independent reporter lines were observed. Confocal images of IRK-GFP localization were obtained for *pub4-1* at 5 dps.

METHODS DETAILS

Vector Construction and Plant Transformation

Transcriptional and translational reporter genes were constructed by standard molecular biology methods and utilizing Invitrogen Multisite Gateway® technology (Carlsbad, USA). Cell type-specific promoters ($pSCR_{2.0}$, pCO_2, and *pWER*) were received in (Gateway compatible) pENTR™ P4P1R or pENTR™ 5′-TOPO® TA vectors from the lab of Philip Benfey, Duke University (Durham, NC, USA). The region 3.1 kb upstream of the ATG of *IRK* (At3g56370) was amplified from Col-0 genomic DNA and recombined into the Invitrogen pENTR™ 5'-TOPO® TA vector. For transcriptional reporters, the pENTR™221-erGFP vector was used as previously described (Van Norman et al., 2014). For translational fusions, the genomic fragment encoding IRK from the ATG up to, but excluding the stop codon (including introns, 3.0kb), was amplified from Col-0 genomic DNA and recombined into the Invitrogen pENTR™ DIRECTIONAL TOPO® (pENTR-D-TOPO) vector. Specific primers for cloning are listed in Table S1. Additionally, pENTR-P2RP3-cGFP vector (Gateway compatible) was used as previously described (Van Norman et al., 2014). The pENTR-P2P3R-YFP-WER3′ entry vector was received from the Benfey lab and used to generate the epidermal transcriptional reporter *pWER:erGFP:WER'3* and the *pWER* driven IRK-YFP reporter (*pWER:IRK:eYFP:WER'3*). Each of the *WER* genomic fragments were as previously described (Lee and Schiefelbein, 1999; Brady et al., 2007). The various Gateway compatible fragments were recombined together with the dpGreen-BarT destination vector (Lee et al., 2006). Expression constructs were then transformed into Col-0 plants by the floral

dip method (Clough and Bent, 1998) using Agrobacterium strain GV3101 (Koncz et al., 1992) and transformants were identified using standard methods. For each reporter gene, T2 lines with a 3:1 ratio of resistant to sensitive seedlings, indicating the transgene is inherited as a single locus, were selected for propagation. These T2 plants were allowed to self and among the subsequent T3 progeny, those with 100% resistant seedlings, indicating the transgene was homozygous, were used in further analyses. For each reporter, at least three independent lines with the same relative expression levels and localization pattern were selected for imaging by confocal microscopy. CRISPR-induced mutagenesis was performed as described in (Fauser et al., 2014), a single guide RNA (5′-ATGG TACTGGGGATGGGGCC) was selected in exon 2 of *IRK*. T2 lines that exhibited a 3:1 ratio of resistant to sensitive seedlings, indicating the CRISPR-guideRNA-containing transgene was inherited as a single locus were selected for continued analyses and sensitive plants were transferred to standard growth media to recover. These plants were subsequently tested for lesions in the *IRK* in proximity to the guideRNA binding site.

Confocal Microscopy and Image Analysis

Roots were stained with ~10 μM propidium iodide (PI) solubilized in water for 1–2 min and visualized via laser scanning confocal microscopy either on a Leica SP8 upright microscope housed in the Van Norman lab or Zeiss 880 microscopes (inverted or upright) housed in the Institute of Integrative Genome Biology Microscopy Core Faculty (UC, Riverside). Root meristems were visualized in the median longitudinal plane and/or stacks of images were acquired in the Z-axis (Z-stacks) and examined with the orthogonal sectioning tool of the LAS X software (Leica) and ZEN (Black Edition, Zeiss). Fluorescence signals were visualized as follows: GFP (excitation 488 nm, emission 492–530 nm), YFP (excitation 514 nm, emission 515–550 nm) and PI (excitation 536 nm, emission 585–660 nm). Alternatively, roots were stained with 10μM FM4-64 (Thermo Fisher) for 5 minutes (excitation at 488nm, detected at 600–660nm). Examination of IRK-GFP expression in Arabidopsis embryos was performed as described in (Crawford et al., 2015). Unless otherwise indicates all confocal images are median longitudinal sections of roots or transverse sections acquired at 6–10 cells above the QC.

scr-4 and *shr-2* mutant seedlings expressing *pCO_2:IRK:GFP* were chosen by visually inspecting root morphology. Median longitudinal sections of *shr-2* and *scr-4* plants expressing *pCO_2:IRK:GFP* were obtained, and GFP intensity across the shootward plasma membrane was measured by using Leica (LAS X) quantification software by generating a line originating at the edge of the GT cell adjacent to the stele and ending at the epidermal edge. The distance from the stele to the epidermis was measured and normalized as a percentage of total, then the location of maximum GFP intensity was recorded in three biological replicates with 6–10 mutant roots per replicate and GFP intensity was measured in 6–8 cells per root. Transverse sections of *shr-2* plants expressing *pCO_2:IRK:GFP* acquired at 500-nm intervals and a representative single section was chosen for the figure. The roots of plants homozygous for either *irk-4 or irk-1* and *pCYCD6;1:GUS:GFP* were examined at 4, 5 and 7 dps. Roots were scored as positive or negative for GFP fluorescence in the endodermis and were then used for longitudinal anticlinal cell division mapping for *irk-1* (details below). In all cases the data shown are from a single biological replicate (of at least three) and similar results were obtained from each biological replicate. Images were analyzed using software accompanying each microscope and assembled into figures in Photoshop (Adobe).

Plasmolysis and Cell Wall Degradation Treatments

The protocol of plasmolysis and partial cell degradation was modified from (Feraru et al., 2011). Briefly, the plasmolysis solution was prepared as following: 0.4M D-Mannitol, 20 mM MES monohydrate and 20 mM KCl, pH to 5.7 adjusted by using 1M Tris-HCl (pH 7.5). To this solution, fresh 10 mM CaCl2 and 3% cellulose was added. For total detachment of the plasma membrane from the cell wall in endodermal cells the incubation lasted one hours and for partial degradation a 30-min incubation was typically used.

Phenotypic Analyses

For phenotypic analysis of Col-0, *irk-1*, and *irk-4*, roots were stained with PI (as described above) and imaged on a Leica SP8 or Zeiss 880 inverted confocal microscope. For phenotypic analysis at 4 dps, Col-0 and *irk-4* seedlings selected from the germination assay (described below) were imaged on a Leica SP8 or Zeiss 880 inverted confocal microscopes. Z-stacks of the root meristem of 11–20 plants for each genotype were acquired for each of three biological replicates. For phenotypic analyses, Col-0 and *irk* mutants were grown side-by-side on 1× MS plates. For analysis at 6 dps of Col-0 and *irk-4*, Z stacks of 11–22 plants for each genotype were taken for each of three biological replicates with a Leica SP8 confocal microscope.

All microscopy analyses done with plants at 4 dps were selected from the germination assay. To assess germination the two genotypes being compared were grown side-by-side on 1× MS plates sealed with parafilm. At 1–2 hour intervals within a time frame of 15–23 hours post stratification, 75–100 seeds were analyzed under a Leica M80 dissecting microscope. Each seed was scored as having imbibed water, seed coat cracked, or emergence of the root (radical) at each time point. Seeds were individually numbered such that the progression of germination over time could be tracked across all the time points. Seedlings of the genotypes being compared, were chosen for subsequent analyses if their germination pattern was the same and they were grown on the same plate. For a particular germination pattern, the same number of seedlings per genotype were analyzed.

To map longitudinal anticlinal and periclinal endodermal cell divisions Col-0 and *irk-4* seedlings selected from the germination assay were imaged by confocal microscopy. Z-stacks of the root meristem of 11–20 plants for each genotype were examined in each of three biological replicates. Longitudinal anticlinal cell divisions (LADs) were observed by analyzing transverse cross sections with the orthogonal sectioning tool of LAS X or ZEN (black edition) software as appropriate. These divisions were placed into one of 8 possible division positions (2 at the xylem pole, 2 at the phloem pole, and 4 between these poles). For each root, beginning at the

QC and moving shootward, the radial position of endodermal LADs was counted in each transverse section (up to 120μm or 15 endodermal cells above the QC). The endodermal or GT cell immediately adjacent to the QC was counted as the first transverse section. The transverse sections were then consolidated into three groups each consisting of a series of 5 transverse sections in the shootward direction (for Figure 5K). The number of endodermal LADs at each of the eight radial positions were then summed for each group. Thus, the maximum possible number of LADs within these groups at a single radial position is five. The number of LADs at a particular radial position for each longitudinal section were added across all roots of a particular genotype in a biological replicate (Figure 5J). Z-stacks of roots expressing *pCYCD6;1:GUS:GFP* in Col-0 and *irk-1* mutant background were examined at 5 dps for each of three biological replicates (n= 8–10). Endodermal LAD mapping of *irk-1* was performed as described above for *irk-4* above.

To examine middle cortex formation in Col-0 and *irk-4*, seedlings at 6 dps were imaged (Leica SP8). Col-0 and *irk-1* seedlings were examined and compared at 7 and 9 dps. Middle cortex was considered present if at least one endodermal cell in the median longitudinal section had undergone a division that appeared periclinal.

To determine the number of persistent CEI in Col-0 and *irk-4* roots, seedlings from the germination assay were examined. Z-stacks were acquired and the orthogonal sectioning tool was used to analyze individual transverse sections just above the QC.

To determine stele area in Col-0 and *irk-4* roots, seedlings from the germination assay were examined. Z-stacks were acquired and the orthogonal sectioning tool was used to analyze transverse sections at 10μm, 60μm, and 120μm from the QC. A polygon was traced along the inner side of endodermal cells and the polygon's area was determined within the relevant software. Width across the xylem and phloem axes were measured at 120μm above the QC.

Movies were created by compiling z-stacks from the phenotypic analyses of Col-0 and *irk-4* roots (6 dps). For one root of each genotype, individual images in the XY plane from the QC to extending shootward 120 μm were exported using the Imaris ×64 9.1.2 software (Oxford Instruments, https://imaris.oxinst.com/). In ImageJ, exported images were grouped, such that arrowheads could be added, and then stacks were created for each group. Lastly, groups of stacks were merged with the hyperstack tool to create one large stack with all of the images for each genotype. These final stacks were saved as an AVI movie with a frame rate of 5 frames per second.

RT-qPCR Analysis

Total RNA for quantitative RT-PCR (qRT-PCR) was isolated using Qiagen's RNeasy Plant Mini Kit. Total RNA was extracted from whole seedlings at 7 dps after growth on our standard growth medium sealed with parafilm. For each of biological replicates, Col-0 and the *irk* allele were grown side-by-side on the same plate. RNA was isolated from each genotype for three independent biological replicates for each *irk* allele. First-strand cDNA was synthesized from 1μg total RNA with RevertAid First Strand cDNA Synthesis Kit and the Oligo$(dT)_{18}$ primer (Thermo Scientific). qRT-PCR reactions were set up using IQ SYBR Green Supermix (BioRad) and analysis was performed on the CFX Connect Real-Time System housed in the Integrative Institute of Genome Biology Genomics Core facility at UC-Riverside. The reaction conditions for each primer pair were: 95°C for 3 min followed by 40 cycles of 95°C for 10 s and 57°C for 20 s. Standard curves were performed at least in duplicate. Primer pair efficiency values were calculated for each replicate of the standard curves and the average efficiency was used for subsequent analysis (Table S1). For each genotype and biological replicate, three technical replicates were performed. Data analysis was performed with the Bio-Rad CFX Manager software 3.1 and transcript levels were normalized to (*PP2A*) (Czechowski et al., 2005).

QUANTIFICATION AND STATISTICAL ANALYSIS

The Leica LAS X software and Zeiss ZEN (Black Edition), as well as ImageJ and Imaris ×64 9.1.2 software (Bitplane, Oxford Instruments, https://imaris.oxinst.com/) were used for post-acquisition confocal images processing. Graphs were generated using Microsoft Excel. The exact value of n, what n represents, the number of biological or technical replicates, the means, standard error of the mean (SEM), standard deviation (SD), and how statistical significance was defined are indicated in each of the relevant figure legends and/or in the STAR Methods details (above). Standard two tailed student's T-test was performed when comparing wild type and mutant phenotypic aspects as a normal distribution is expected.

DATA AND CODE AVAILABILITY

This study did not generate or analyze any large-scale datasets. Original confocal micrographs are available upon request from the Lead Contact.

Developmental Cell, Volume *52*

Supplemental Information

The Arabidopsis Receptor Kinase IRK Is Polarized and Represses Specific Cell Divisions in Roots

Roya Campos, Jason Goff, Cecilia Rodriguez-Furlan, and Jaimie M. Van Norman

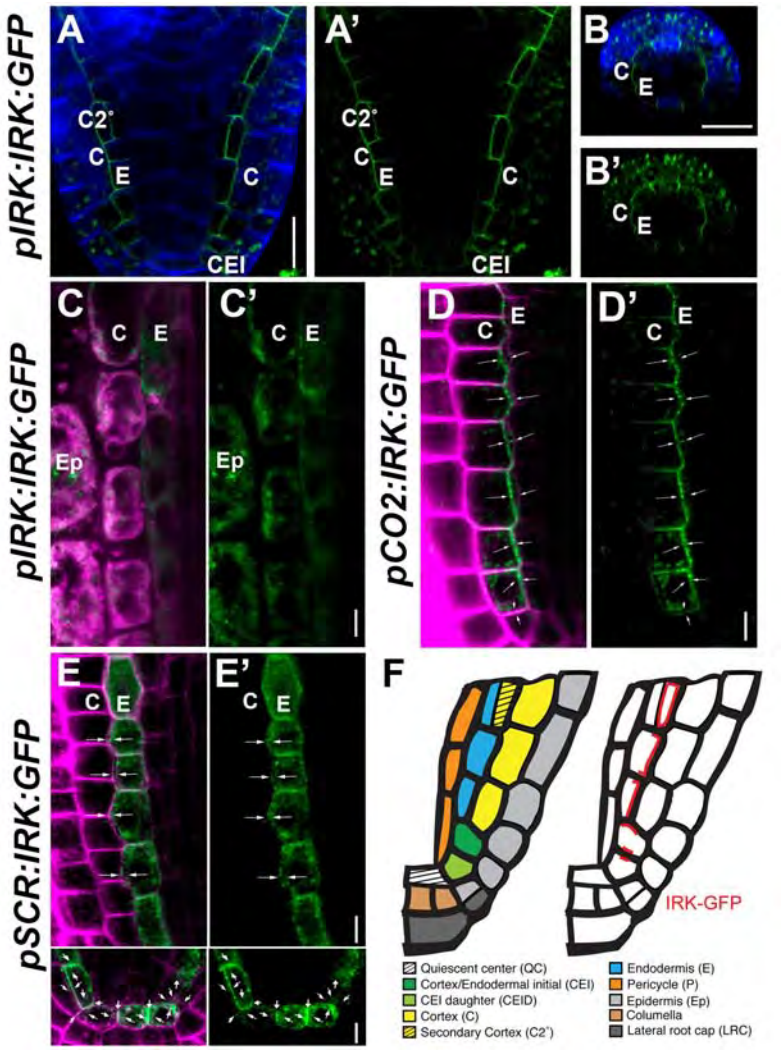

Figure S1. IRK-GFP is polarly localized in the embryonic GT and closely interacts with the cell wall in the cell wall, related to Figures 2 and 3. (A-E) Confocal images of roots expressing IRK-GFP (green) and stained with SR2200 dye (blue) or the membrane tracer FM4-64 (magenta); side-by-side panels show images with dye+GFP merged (α) and GFP alone (α'). (A) Median longitudinal section of the hypocotyl and root portion of an early torpedo stage embryo expressing *pIRK:IRK:GFP,* and (B) transverse hypocotyl section from the same embryo. (C-E) Plasmolysis with partial degradation of the cell wall in roots expressing (C) *pIRK:IRK:GFP,* (D) *pCO2:IRK:GFP,* and (E) *pSCR:IRK:GFP*. (C) IRK-GFP polar distribution is lost and signal is detected in both endodermal and cortex cells indicating that the fluorescence observed at the plasma membrane reflects signal from both cell layers. (D) IRK-GFP signal in the cortex is observed at the inner PM domain and we detect IRK-GFP in strands of partially detached PM (white arrows). (D) In the endodermis, IRK-GFP is observed at the outer PM domain and at cell wall-PM interface (white arrows). In QC cells and ground tissue cells immediately adjacent to the QC (lower panels), IRK signal is similarly detected in PM that is partially detached from the cell wall with polarity indicated in each cell (white arrows). (F) Schematic of median longitudinal section of embryonic root/hypocotyl showing cell types and IRK-GFP accumulation (red). Abbreviations for cell types: endodermis (E), cortex (C), secondary cortex (C2˚), cortex/endodermal initial (CEI), and epidermis (Ep). Scale bars: (A-B) 25μm, (C-E) 5 μm.

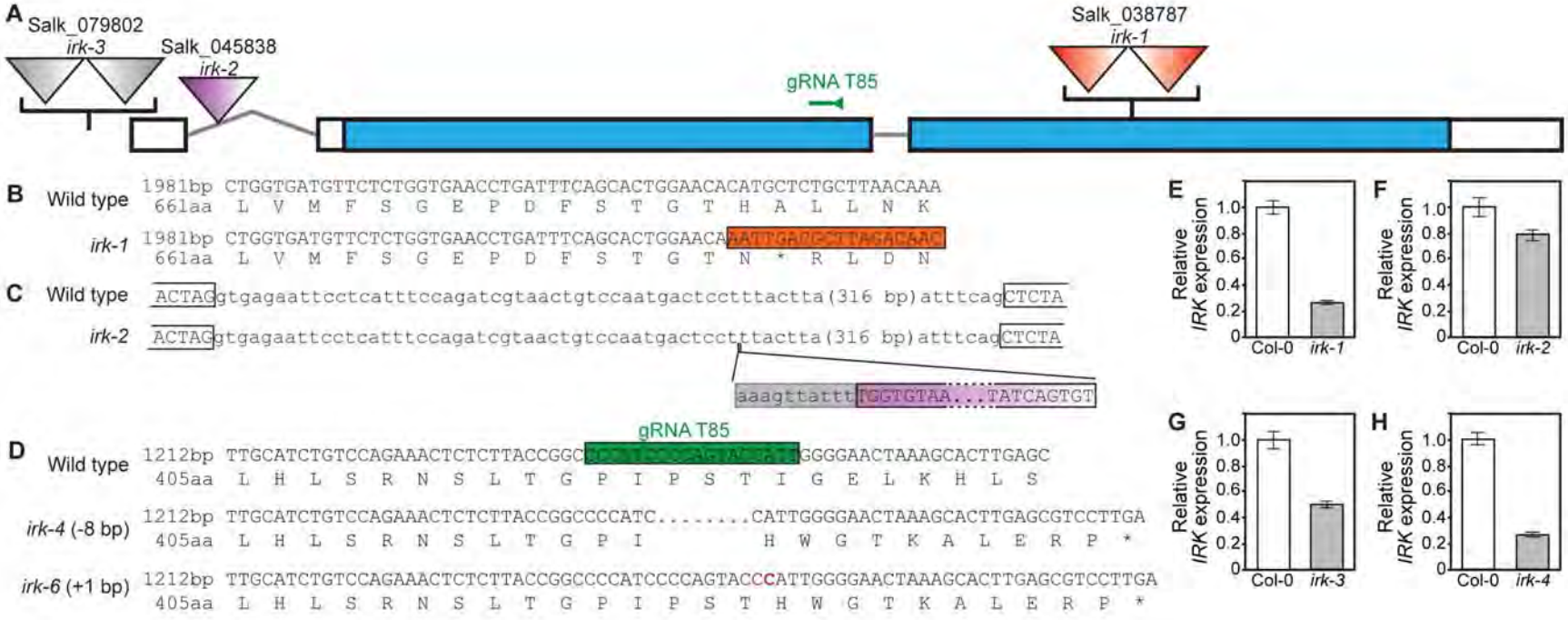

Figure S2. *IRK* gene structure, mutant alleles, expression analyses, related to Figure 5. (A) *IRK* gene model (⅞ scale) with untranslated regions (white boxes) and coding regions (blue boxes). Publically available T-DNA alleles (triangles) and the guide RNA (gRNA, green) used to generate CRISPR-induced alleles (not to scale) are shown. T-DNA positions were identified by sequencing; left borders are indicated by darker shading and right borders are indicated by lighter shading. For *irk-1 and irk-3,* multiple copies (at least 2) of the T-DNA are inserted with the outermost T-DNAs mirrored, such that left border sequence is present on both sides of the lesion. The *irk-3* insertion occurs 110 bp upstream of the predicted transcriptional start site. (B-D) Select portions of the *IRK* coding and amino acid sequences for WT and *irk* mutants. Numbers indicate base pairs (bp) and amino acids (aa) from the start codon. (B) The *irk-1* insertion (orange triangles in (A) and boxed region) is located in exon 3 and results in a premature stop codon (asterisk), which likely truncates the protein after 676aa (full length IRK is predicted to be 964aa). (C) The *irk-2* insertion (purple triangle in (A) and boxed region is located in the first intron 44 bp downstream of exon 1. This insertion also includes 10 bp of unknown origin (gray box). (D) Two CRISPR-induced alleles were isolated from WT (Col-0) plants expressing CRISPR-Cas9 and gRNA T85. The *irk-4* and *irk-6* alleles have an 8-bp deletion and 1-bp insertion, respectively, which ultimately result in premature stop codons (asterisks). These two alleles had similar mutant phenotypes, and we focused our studies on *irk-4*. (E-H) *IRK* expression relative to Col-0 in the different *irk* alleles. The graphs show the average of three biological replicates and error bars indicate SEM. Expression of *IRK* is lowest in (E) *irk-1* and (H) *irk-4* when compared to Col-0.

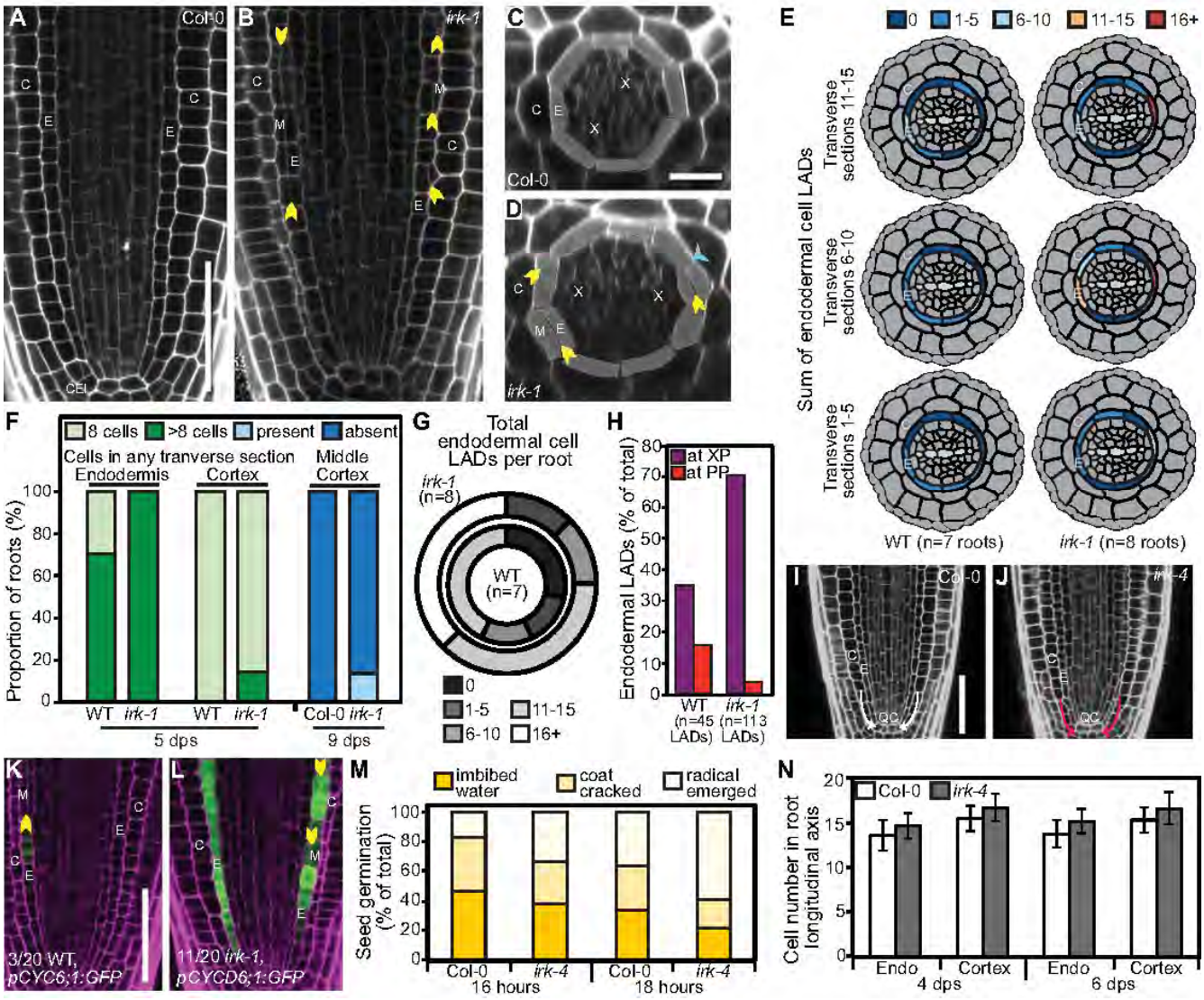

Figure S3. Abnormal root phenotypes of *irk* mutants, related to Figure 5 and Table 1. (A-D) Confocal micrographs of WT and *irk-1* (at 6 dps) with endodermal periclinal and longitudinal anticlinal cell divisions indicated by yellow and cyan arrowheads, respectively. Note endodermal cells and all daughter cells traced and highlighted to increase visibility. (E-H) Phenotypic data from one biological replicate (of three) per genotype (n= 7-8 roots at 5 dps), excluding middle cortex, which was assessed at 9 dps (n=22-24 roots). (E) Schematics summarizing the number of endodermal LADs at specific positions (xylem axis in light grey) in serial sections above the QC. (F) Bar graph summarizing *irk-1* phenotypic aspects (note: WT plants are also expressing *pCYCD6;1:GUS:GFP*). (G) Donut chart showing total number of endodermal LADs per root and (H) bar graph showing the proportion of these divisions at the vascular poles. (I, J) Confocal micrographs (6 dps) showing the position of GT cell layers. (I) Col-0, the GT aligns with the QC (white arrows), whereas in ~5% of *irk-4* (J), the GT doesn't align with the QC (red arrows). (K, L) Confocal images of roots (at 7dps) expressing *pCYCD6;1:GUS:GFP* (green) stained with PI (magenta). (K) In WT, *pCYCD6;1* activity is observed in endodermal cells with adjacent to those that have divided to form middle cortex, however, in *irk-1* more endodermal cells express *pCYCD6;1* . (M) Bar graph showing stages of germination at hours after stratification. (N) Bar graph showing endodermal and cortical cell number (from QC up to 120 µm) in the median longitudinal axis as a measure of transverse anticlinal cell divisions (n=17-20 roots/genotype). Data from one biological replicate in which cell numbers in Col-0 and *irk-1* were the most different. Abbreviations: quiescent center (QC), cortex/endodermal initial (CEI), endodermis (E), cortex (C), middle cortex (M), xylem axis (X), xylem pole (XP), and phloem pole (PP). Scale bars: 50 µm (A, B, I, J), 100 µm (K, L) and 20 µm (C, D)

Table S1. Cloning and genotyping primers, related to Figures 2, 3, 4, and S2.

Purpose	Primer name	Sequence (5'-3')
Genotyping	Salk_038787_LP	TCCATCAAGAATTGCAGTTCC
	Salk_038787_RP	CCTCGCTAATCCGTAGTCTCC
	Salk_045838_LP	CCAGACAAGCCATTGCTACTC
	Salk_045838_RP	AAATAAAAGCCACGTGTCAGC
	Salk_079802_LP	ATTCAACCGCATTTCAATCTG
	Salk_079802_RP	TTCAACCTTCAAGTGAATGGC
	LBa1	TGGTTCACGTAGTGGGCCATCG
	370_8bpdel_WT_F	TTACCGGCCCCATCCCCAGTAC
	370_8bpdel_MUT_F	TACCGGCCCCATCCATTG
	370trunc_R2	TACTGCTGATCTTGAAACCGT
	scr-4_mutF3	CTTATCCATTCCTCAACTCTATT
	scr-4_F3	TTATCCATTCCTCAACTTCAGT
	scr-4_R3	TGGTGCATCGGTAGAAGAATT
	shr-2_F	TCTCCATACCTCAAACTCCTCC
	shr-2_R	TTGCCTCTCCGTCTACTGC
	Salk_108269_LP	CAAGACTCGACAGACCCTGAC
	Salk_108269_RP	AATTCTCCTTGGCTTCAGAGC
Cloning	56370cod_F	CACCATGTACAAAGCACTGATTTTTACAGTC
	56370cod_R	ACTTGAACCCAACTCATCTGAG
	56370pro_F	CACAGCCCTTATTCATCTCCTAC
	56370pro_R	CTTTCCACAACCCTCTTCTCC

Table S2: Primers and primer efficiency information for qRT-PCR, related to Figures 5 and S2.

		Primer Efficiency (%)					
Primer name	**Primer sequence 5' -> 3'**	**Run 1**	**Run 2**	**Run 3**	**Run 4**	**Run 5**	**Average**
PP2A_qF	TAACGTGGCCAAAATGATGC	97.7	95.7	97.9	96.7	97.0	97.0
PP2A_qR	GTTCTCCACAACCGCTTGGT						
370_ex2_qF2	GGTGGAGCTGTTTCTTTGGA	91.5	88.5	86.4	ND	ND	88.8
370_ex3_qR2	GGTGGAATTGAGCCTAGCAG						
370_ex1_qF2	CTGCAACATTCTTCGTCGGAAATC	90.3	86.6	75.8	ND	ND	84.2
370_ex2_qR4	GCTCTGGATCTCGTAAATCGGCTT						
370_ex1/2_qF1	TCTTACTAGCTCTACATAACTGAAA	95.1	96	ND	ND	ND	95.6
370_ex2_qR5	GGCGGGTCTAGAGATCTCAC						
370_ex2/3_qF1	CCTTCGGTCTTTGATCCTGTC	90.1	90.6	ND	ND	ND	90.4
370_ex3_qR3	TGAAGATAGCCGAGATTAGCCA						